Study of Ion and Solvent Transport through Graphene Oxide Membranes

by

Kai Wang

A thesis

presented to the University of Waterloo

in fulfillment of the

thesis requirement for the degree of

Master of Science

in

Chemistry

Waterloo, Ontario, Canada, 2016

Author's Declaration

I hereby declare that I am the sole author of this thesis. This is a true copy of the thesis, including any required final revisions, as accepted by my examiners.

I understand that my thesis may be made electronically available to the public.

Abstract

Filtration membranes are required to be thin, robust, energy efficient, and accurate on selectivity. Graphene oxide (GO) is believed to be a potential next generation material for industrial membrane applications because of its unique properties such as strong mechanical strength, excellent aqueous solution processability, and great flexibility for membrane fabrication. Research on the transport models, the separation performance, and the functionalization of GO membranes has been developed. However, many mechanisms of mass transport through GO membranes still remain debatable.

In this work, GO was synthesized, and then functionalized with linear amine-terminated poly(ethylene glycol) (PEG) and aluminum ions (Al). The fabrication and characterizations of GO, PEG-GO, and Al-GO membranes were demonstrated in this work. Water and water/ethanol binary mixture transport through GO, PEG-GO, and Al-GO membranes were studied to investigate the permeation and the rejection rates of solvents through GO-based membranes. The total volumetric flux of water/ethanol mixture through GO membranes was inversely proportional to the viscosity of the solvent mixtures. The steric hindrance effect and the interactions between the solvent molecules and the membrane surfaces dominated the rejection rate of ethanol through GO membranes. The functionalization of GO modified the pore size and the porosity of the membranes, resulting in faster permeation of solvents and reduced rejection rates of ethanol through PEG-GO and Al-GO membranes. Deformation of nanochannels within the functionalized GO membranes was observed when the membranes were operated under highly pressurized conditions. Diffusive transport of two charge equivalent and structurally similar ruthenium complex ions $Ru(bpy)_3^{2+}$ and

Ru(phen)$_3^{2+}$ through GO, PEG-GO, and Al-GO membranes were also studied. Our data showed high similarity with the results reported previously in the literature, indicating that the GO and functionalized GO membranes used in this work were highly consistent. Due to the enlarged pore sizes and the reduced interactions between ions and the membrane surfaces, the flux of ions through PEG-GO membranes was 300% higher than that through GO membranes. In contrast, permeation of ions through Al-GO membranes was slower than that through GO membranes. The blocked nanopores and the electrostatic repulsion between the intercalated aluminum ions and complex ions were the main reasons for this observation. In addition, the main reason for the significant permeance difference between Ru(bpy)$_3^{2+}$ and Ru(phen)$_3^{2+}$ ions was confirmed as the steric hindrance effect.

This work contributes to the basic research on GO membranes in potential applications. It can be beneficial to the academic laboratories for understanding the mechanism of mass transport through GO-based membranes. These new membrane materials could replace traditional membrane materials in many industrial applications in the future.

Acknowledgements

First of all, I would like to express my sincerest gratitude to my supervisor, Dr. Shirley Tang for her patience, enthusiasm, and continuous support of my MSc study and research. With the great opportunity that she provided me over the past two years, I was able to study and work in a warm group, and further my knowledge in chemistry.

Besides my supervisor, I would like to thank the rest of my thesis committee: Dr. Xianshe Feng, Dr. Vassili Karanassios and Dr. Jean Duhamel for their encouragement and assistance.

Finally, I would like to thank past and present members of Dr. Shirley Tang's research group, including Mike Coleman, Dr. Samaneh Shadmehr, Zhi Li, Yun Wu, Louis Cheung, Xiguang Gao, Andrew Wenger, Marvin Jiang, Yuan Gao, Gaganprit Gill, Yael Zilberman-Simakov, Yuxing Wang, and Irfani Ausri.

Table of Contents

List of Tables

List of Figures

List of Abbreviations

AFM: Atomic Force Microscopy

Al-GO: Aluminum Ion Intercalated Graphene Oxide

bpy: 2,2'-bipyridine

CNT: Carbon Nanotubes

DLC: Diamond-like Carbon

DLS: Dynamic Light Scattering

EDAX: Energy-dispersive X-ray Spectroscopy

EDC: 1-Ethyl-3-(3-dimethylaminopropyl) carbodiimide

EDL: Electrical Double Layers

FTIR: Fourier Transform Infrared Spectroscopy

GO: Graphene Oxide

HP: Hagen-Poiseuille

MES: 2-(N-morpholino)ethanesulfonic acid

MFR: Molar Flow Rate

MWCO: Molecular Weight Cut Off

NHS: N-hydroxysuccinimide

PDMS: Polydimethylsiloxane

PEG: Polyethylene Glycol

PEG-GO: Polyethylene Glycol Functionalized Graphene Oxide

phen: 1,10-phenanthroline

SEM: Scanning Electron Microscopy

SWCNT: Single-walled Carbon Nanotube

TGA: Thermogravimetric Analysis

UV-vis: Ultraviolet-visible Spectroscopy

XRD: X-ray Diffraction

Chapter 1   Introduction

Membranes work as selective barriers that allow certain kinds of particles to pass through, and block others. It is widely used in water treatment,[1-3] food production,[4-5] fuel cells,[6-7] gas separation,[8-10] and other industrial applications.[85] The particles that travel through the membranes can be ions, gas molecules, solvent molecules, bio-macromolecules, etc. Depending on the substance that travels through the membranes and the corresponding applications, the membrane characteristics and underlying mechanisms can be drastically different. However, some membrane properties such as high permeance, excellent robustness, and high selectivity are commonly desired.[11]

Graphene Oxide (GO) which is a derivative of graphene is a new type of carbon-based membrane material. The unique properties of GO such as good aqueous solution processability, 2-dimensional (2D) structure, strong mechanical strength, excellent flexibility, and tunable functionalities have been widely discussed. These advantages of GO enable GO membranes to be thin enough, robust enough, energy efficient, flexible and suitable for large-scale fabrication, and therefore, match the basic requirements for industrial use. GO membranes have also shown great potential in specific applications such as water purification and gas separation. It is believed that GO membranes can enable many potential applications in the future.[12-13, 48] This chapter introduces the properties of GO and the mechanisms governing mass transport through different types of GO membranes.

1.1 Mass Transport through Membranes

Mass transport through membranes happens every second and everywhere in this world. Oxygen travels through the red blood cell membrane and binds to hemoglobin.[14] The reverse osmosis plant membrane system enables low energy consumption water desalination.[15] Alcohol and milk can be pressed through polymeric membranes for dehydration.[16] Various driving forces, including pressure, temperature, chemical potential, and electrical potential are utilized to drive particles, including ions, gas molecules, solvent molecules, etc. to pass through membranes.[17] Depending on pore size, filtration membranes can be classified as microfiltration membranes, ultrafiltration membranes, nanofiltration membranes, and reverse osmosis membranes.[33] Because of its attractive properties such as low energy consumption and high flux rate, nanofiltration membranes have replaced traditional membranes in many applications.[67]

GO membranes have a well-defined nanoporous structure, and it is anticipated to be suitable for many nanofiltration applications. Since ultrafast pressure-driven separation membranes are becoming very important in the industry, this work investigates pressure-driven solvent transport through GO membranes. In addition, because many commercial applications require membranes to have good ion separation performance, ion transport through GO membranes is also studied. Therefore, mass transport driven by both pressure and chemical potential are discussed in this chapter.

1.1.1 Pressure-driven Solvent Transport through Membranes

Nanofiltration membranes have gained much interest over the past several years. Research on transport performance, modeling, and mechanisms of nanofiltration membranes have been carried out extensively.[57-61, 86-90]

The Hagen-Poiseuille (HP) model is the most commonly used model for estimating the flux of aqueous solution through hydrophilic membranes,

$$J = \frac{\varepsilon r^2}{8\mu\tau}\frac{\Delta P}{\Delta x} \tag{1.1}$$

where J is the solvent flux, and ΔP is the applied pressure. The rest of the parameters, including porosity ε, pore size r, tortuosity τ, and thickness Δx of the nanofiltration membranes, describe the influence of the membrane properties on the solvent flux. The only parameter related to solvent property is μ, which is the viscosity of the solvent. Although the interaction between membranes and solvent molecules are not considered in this model, it has been proven that the HP equation works well with hydrophilic membranes, and has been extensively used in many studies to estimate mass flux through membranes.[11, 64-66, 68]

As described by Equation 1.2, Geens and coworkers reported a transport model that integrates three most important parameters in transport phenomena through nanofiltration membranes.[62]

$$J \sim \frac{V_m}{\mu \cdot \Delta\gamma} \tag{1.2}$$

where J is the solvent flux, V_m is the molar volume of solvent molecules, μ is the viscosity of solvent, and $\Delta\gamma$ is the surface tension difference between the liquid solvent and the solid membrane surfaces. First, as the most common parameter that appears in all transport models, the solvent viscosity μ measures the resistance against the pore flow. Second, the molar volume represents the

size of the solvent molecules. Obviously, regardless on whether mechanism of transport is convection or diffusion, increasing molecular size causes a greater steric hindrance and a decreased diffusivity, resulting in a reduced transport flux. At last, the surface tension difference $\Delta\gamma$ is related to the interactions between the membrane surfaces and the solvent molecules. Surface tension of a membrane can be determined by measuring the contact angle, and the surface tension of a liquid can be calculated based on the mixing rule for aqueous solutions. Transport of binary water/ethanol mixtures through different hydrophilic and hydrophobic membranes was tested to evaluate the new model developed by Geens et al.[63] Similar to the HP model, the estimated results matched the experimental results very well for hydrophilic membranes. However, the new model was shown to give more accurate predictions compared to the HP model for transport through hydrophobic membranes. The difference between these two models was attributed to the solvent-membrane interactions. Since water and ethanol have relatively high polarity, this binary mixture showed strong affinity to the hydrophilic membranes, thus resulted in weak repulsion between solvent molecules and the membrane surface. Therefore, the influence of solvent-membrane interaction on mass transport was not significant. In comparison, the solvent-membrane repulsion in the case of hydrophobic membranes increased considerably, leading to a decrease in the flux of the binary solvent mixture. Since the HP model does not take membrane-solvent interactions into consideration, it is less accurate than the new model.

In another report given by Geens et al.,[69] the partial flux of ethanol/water mixture transport through hydrophilic, hydrophobic, and semi-hydrophilic nanofiltration membranes was calculated and analyzed. First of all, the experimental results indicated that the bulk properties of ethanol/water mixtures can be applied in the analysis, and the flux of solvent through nanofiltration membranes should be analyzed based on convective transport models instead of diffusive models.

Not only that, it is observed that the flux of ethanol/water mixtures through hydrophilic membranes was obviously greater than the flux through hydrophobic membranes. Adding ethanol into pure water caused an obvious decrease in the polarity of the solvent mixtures, and a dramatically reduced partial water permeation rate through hydrophobic membranes was then observed. In contrast, adding water into pure ethanol did not change the polarity of the solvent mixtures significantly. Both partial permeation rates of ethanol and water through hydrophilic membranes were very low at high ethanol molar percentages. For hydrophobic membranes, by contrast, low partial permeance of both ethanol and water were observed at low ethanol molar percentages, and relatively high permeability was observed at high ethanol molar percentages. The surface tension difference between membranes and solvents gives a credible explanation for the huge difference between the fluxes of ethanol/water mixture through hydrophilic and hydrophobic membranes. That is, besides solvent viscosity, the interaction between the membrane surfaces and the solvent molecules is proven to have a great influence on the permeability of solvents through membranes. The main purpose of the model reported by Geens *et al.* was to correct the theoretical calculations for transport of polar solvents through hydrophobic membranes. Without considering the solvent-membrane interaction, the HP model should still be adequate to analyze the transport of polar solvents through hydrophilic membranes.

1.1.2 Ion Diffusion

Ion separation is crucial for many applications such as water purification and seawater desalination. This chapter focuses on the ion diffusion phenomenon driven by chemical potential without other external influences. The flux of ion diffusion along a given direction can be expressed by Fick's First Law:[97]

$$J = -D\frac{dC}{dx} \tag{1.3}$$

where J is the flux, D is the diffusion coefficient, C is the ion concentration, and x is the direction of diffusion. Accordingly, the equation below can be used to determine the molar flow rate (MFR) of ions through a GO membrane:[30]

$$MFR = D\Delta C\frac{A_e}{L_e} \tag{1.4}$$

$$A_e = A \cdot \frac{d}{L} \tag{1.5}$$

$$L_e = L \cdot \frac{h}{d} \tag{1.6}$$

where ΔC is the concentration difference across the membrane, A_e is the effective membrane area, L_e is the effective path length of the ions, d is the interlayer space within a GO membrane, A is the area of the membrane surface, L is the average lateral size of individual GO flakes, and h is the thickness of a GO membrane.[25]

The bulk diffusivity and the Stokes-Einstein radius can be determined by the Wilke-Chang equation (Equation 1.7) and the Stokes-Einstein equation (Equation 1.8):[91-96]

$$D = \frac{7.4 \times 10^{-8} T \sqrt{\alpha_v M_v}}{\eta_v V_o^{0.6}} \tag{1.7}$$

$$D = \frac{k_B T}{6 R_s \pi \eta} \tag{1.8}$$

where D is the bulk diffusivity, T is temperature, α_v is the association coefficient, M_v is the molecular weight of solvent molecules, η_v is the viscosity of solvent, V_o is the molar volume of solute at its normal boiling point, k_B is the Boltzmann constant, η is the viscosity of the ion solution, and R_s is the hydrodynamic radius (Stokes-Einstein radius) of the ions under the assumption that the ions behave like hard spheres.

1.2   Membrane Materials

With the development of industry, a few important membrane properties are commonly desired for new advanced membranes. First, the membranes should be thin enough to maximize the permeance, therefore, saving as much energy as possible. Second, the membranes should be robust enough to deal with the caustic and high pressure environment, therefore, maintaining good performance for a longer time. Third, the membranes should also have well-defined pore size to keep the selectivity accurate and stable. At last, the production cost of the membranes should be relatively low, therefore, being suitable for large-scale fabrication.[11]

By far, polymeric membranes are used on large scales commercially.[18-19] They showed good separation performance for gas separation (for instance, separate nitrogen gas from air) and sea water desalination. Polymeric membranes are suitable for mass production as well. However, when polymeric membranes are applied under special working conditions such as high temperature, high pressure, and corrosive media, the channels within membranes are relatively easy to be compressed or chemically corroded, causing reduced permeance and unstable rejection rates.

Compared to polymeric membranes, ceramic membranes show better stability, comparable permeance and rejection rates with excellent chemical resistance. However, because ceramic

7

membranes are expensive and fragile, they are not suitable for large-scale production and industrial use.[20]

Recently, carbon-based membranes attracted researchers' attention. Hummer *et al.* initially used carbon nanotube (CNT) as the main material to fabricate nano-filtration membranes.[21] It is found that water molecules in the single-walled carbon nanotube (SWCNT) can form a one-dimensional hydrogen-bonded chain. Because the hydrophobic wall of CNT does not affect the hydrogen-bonded water chain, water flow through CNTs is much faster than other nano-filtration systems.[22] Furthermore, the open ends of a CNT make it possible to be modified with a polymer, protein, DNA, etc. to match specific selectivity requirements. Also, CNTs are well known for their strong mechanical strength and good chemical resistance. However, producing dense vertically aligned CNTs on a large scale is still a technical challenge which limits the widespread use of CNT membranes.

Besides CNTs, diamond-like carbon (DLC) is regarded as another carbon-based material that can be made into membranes.[24] It showed good organic solvent separation performance.[23] DLC has great mechanical strength, with a Young's modulus only ten times smaller than diamond. However, DLC membranes have the same problem as ceramic membranes. The cost of production of DLC membranes is too high for economic production and industrial use.

The third carbon-based membrane material is graphene-based materials. Graphene is a one-atom-thick film of sp^2-bonded carbon atoms.[25] Since graphene was discovered in 2004 by Dr. Andre Geim at Manchester, it has attracted huge world attention because of its unique properties such as high mechanical strength, strong chemical resistance, and it two-dimensional structure. However, large scale production of graphene is still not available yet. In comparison, GO, which is a chemical derivative of graphene, appeared to be an economic alternative. GO has the same

two-dimensional structure as graphene. Because of the harsh oxidation condition used during the synthesis process, GO contains mainly three types of oxygen-rich functional groups: hydroxyl, carboxyl, and epoxy groups, decorating on the graphitic basal plane and its edges.
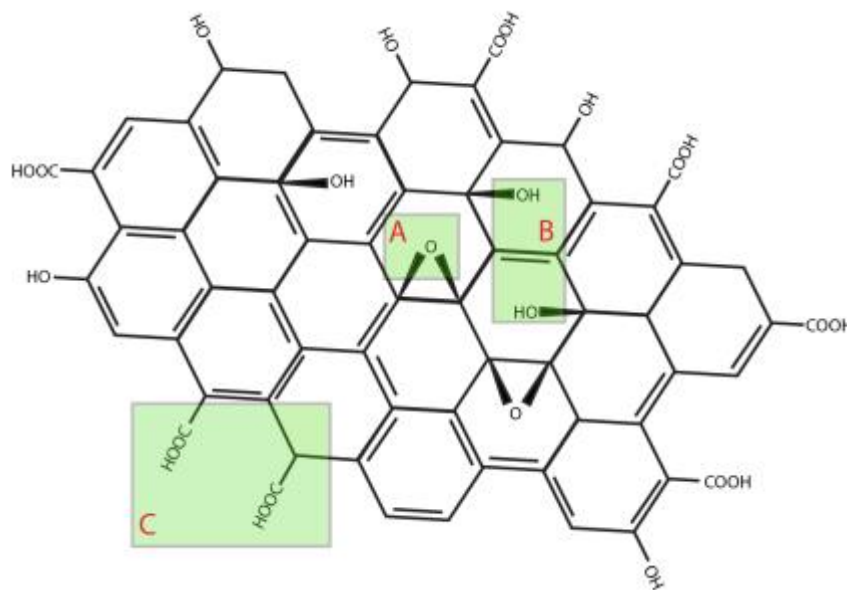
Figure 1.1 Chemical structure of GO. A, B, and C correspond to epoxy, hydroxyl, and carboxyl groups.

GO has a few advantages over graphene. First, because of the hydrophilic carboxyl and hydroxyl groups, GO has good aqueous solution processability. Therefore, GO membranes are more suitable for large scale production than graphene. Second, because no extra organic solvent is needed in the membrane fabrication process, GO membranes are more environmentally friendly. Third, when GO flakes are made into membranes by vacuum filtration,[32,70] spin coating, or layer-by-layer assembly method,[37] hydrogen-bonds would form between adjacent GO flakes, resulting

in good mechanical strength of GO membranes.[27] Furthermore, the functional groups can deprotonate in aqueous solutions, and the electrostatic repulsion between the negatively charged functional groups 'support' the weight of adjacent flakes, thus creating interlayer nanochannels within GO membranes. These naturally formed well-defined nanochannels are the key to the GO membranes' transport performance. At last, these oxygen-containing functional groups make it easy to functionalize GO flakes with polymer, DNA, and others to further tune interlayer channel size. Based on these advantages, GO membranes are believed to have the potential to enable many applications in the future.

1.3 Graphene Oxide Membranes

1.3.1 Fabrication and Structure of GO Membranes

Because of the oxygen-containing functional groups on GO flakes, GO has good processability and solubility in aqueous solutions. Therefore, the most common GO membrane fabrication methods, including drop-casting,[31] layer-by-layer assembly,[37] vacuum filtration method,[11,32] and pressure filtration method use aqueous GO solutions to make membranes. Although GO membranes can be fabricated with different methods, the GO flakes would finally stack together and form similar nanoporous structures in GO membranes.

As shown in Figure 1.2, the cylindrical pores and slits are the two main types of pore structures in GO membranes. First, the cylindrical pores are generated by vacancies and cracks within individual GO flakes, and voids between individual GO flakes. The vacancies and the cracks are created by the exfoliation and oxidation processes during GO synthesis, while the voids are formed by the misalignment of GO flakes during the GO membrane fabrication process. The

length of these cylindrical pores is shorter than 5 nm. Second, the slits are the interlayer spaces between adjacent GO flakes. The size of these 2D nanochannels is only around 0.4 nm when GO membranes are in the dry state. Because the oxygen-containing functional groups on GO flakes can absorb water molecules and swell in aqueous solutions, the interlayer space can be enlarged to 1.4 nm when GO membranes are fully hydrated.[31, 114]

Figure 1.2 Schematic drawing of the pore structures in GO membranes: (A) Cylindrical pores; (B) Slits.

The porosity and the pore size of GO membranes are important factors determining the permeation and rejection rates of particles through GO membranes.[11,31-36] For instance, it is found that ion diffusion is mostly facilitated by cylindrical pores in thin GO membranes, while slits become dominant in thick GO membranes.[32] Because the ions that permeate through GO membranes are hydrated in aqueous solutions, it is reasonable to assume that permeation of polar solvents such as water and ethanol through GO membranes should follow the same rule mentioned

above. Recent studies on the mechanisms of ion and solvent permeation through GO membranes are reviewed in the following sections.[73-79]

1.3.2 Ion Selectivity of GO Membranes

Ion selectivity of GO membranes is critical to many potential applications of GO membranes such as sea water desalination, food production, and drinkable water purification. Joshi *et al.* investigated the permeation of different ions through micrometer-thick GO membranes in aqueous solutions.[30] GO membranes blocked all solutes with hydrated radius greater than 4.5 Å. That is, the size effect dominated the ion selectivity of the GO membranes. The permeance of small ions such as Na^+, K^+, and Cl^- through the GO membranes was found to be thousands of times greater than what is expected for simple diffusion. The charges of the ions did not affect the permeation rate. The capillary force acting on ions within the nanochannels was regarded as the main reason for this fast permeation.

Similarly, Sun *et al.* measured the permeation rates of different ions through the GO membranes. They found that small metal ions can travel through GO membranes smoothly, while heavy metal ions normally have a much lower permeation rate. Because the stacked-layers structure within GO membranes stayed closed when the membranes were still in the dry state, no permeation of ions was observed in the first several hours. After that, the hydrophilic oxygen-containing functional groups on GO flakes started to absorb water molecules and swell. As a result, the interlayer space was enlarged and allowed hydrated ions to pass through. At this stage, the size effect dominated the ion diffusion through GO membranes. As a result, the permeation rate of Na^+ was much greater than some heavy metal ions such as Mn^{2+}, Cd^{2+}, and Cu^{2+}. However, the permeation rates of the heavy metal ions such as Mn^{2+}, Cd^{2+}, and Cu^{2+} through GO membranes

were mainly determined by their different coordination conformations and complex reactions. Therefore, besides the size effect, the interactions between ions and GO membranes such as chemical reactions, electrostatic forces, and π-π stacking interactions are also important factors determining the permeation rates of ions through GO membranes.[31]

1.3.3 Solvent Permeation through GO Membranes

Although GO is itself an excellent gas barrier that blocks 99% of H_2, N_2, He, and vapors of many organic solvents under relatively low pressurized conditions, completely different results were observed for solvent transport through GO membranes.[27-29] As the most common solvent used in industry, water transport through GO membranes received significant attention in recent years. A lot of research showed that water can permeate through GO membranes with rates much higher than many commercial ultrafiltration membranes.[30,37-38] The flow enhancement is attributed to the capillary force acting on water molecules in the nanochannels. Another explanation for this ultrafast water flow is that water molecules prefer to travel through the hydrophobic non-oxidized regions on GO flakes as a frictionless flow. The continuous changing of hydrogen bonded water molecules makes water flow smoothly and fast.[45-47]

As mentioned in the previous section, the pore size of GO membranes is an important factor determining the permeation of water through GO membranes. Besides the swelling effect of the oxygen-containing functional groups, the pressure applied to the system, the pH value and the concentration of the solution are able to affect the channel size of GO membranes as well.[11] At the beginning, when GO membranes are hydrated, the hydroxyl and carboxyl groups on GO flakes can react with water and deprotonate, thus becoming negatively charged. The electrostatic repulsion between adjacent GO sheets forces the closely stacked layers to separate, therefore

enlarging the interlayer space. A relatively high permeation rate of water would be observed. When salt is added into the solution, an electrical double layer (EDL) would form and screen the electrostatic forces between adjacent layers, thus causing a reduction of the interlayer space. Consequently, the permeation rate of water through GO membranes would decrease. Similar results would be observed if acid was added to the aqueous solution. As the surrounding pH value is lowered, reactions between the functional groups and protons would become more active. The net negative charges on GO flakes would decrease, and the interlayer space would be reduced. In addition, the nanochannels in GO membranes can be compressed under high pressurized conditions, therefore resulting in a lower flux of water.

With respect to the permeation of solvent mixture through GO membranes, Geens *et al.* believed that viscosity and polarity of the mixtures are the solvent properties with the largest influence.[69] Because of the oxygen-containing functional groups, GO membranes have good hydrophilicity. As a result, polar solvents such as water and ethanol have higher permeance than nonpolar solvents. Besides the pure GO membranes, GO can also be added into polymeric membranes to improve the hydrophilicity of the membranes. An obvious enhanced water flow was observed by Ganesh and coworkers.[39] Huang *et al.* proved that the flux of water/ethanol mixtures through GO membranes was inversely proportional to the viscosity of the binary solvent mixture in their experiments.

In conclusion, besides the membrane parameters such as thickness, porosity, and size of the nanochannels in GO membranes, solvent polarity and viscosity, and environmental factors including pressurized conditions, and solution concentration and pH are able to affect the permeation of solvent through GO membranes.

1.4 Strategies to Functionalize GO Membranes

Functionalization of GO membranes can modify the porous structure within GO membranes. As a result, it can reinforce the mechanical strength of GO membranes, and/or improve the permeance and the rejection rate of particles through GO membranes. Three promising strategies to functionalize GO membranes are discussed in this section.[80-84]

First, nanopores can be directly introduced onto GO flakes. Electron beams can be used to punch holes in the GO sheets, and KOH can be applied to chemically activate the microwave-exfoliated GO to produce nanopores as well.[40,41,107] The nanopores produced with this method had a similar size as the original nanochannels within the GO membranes. The formation of these nanopores greatly shortened the length of the path that particles needed to travel through within a membrane. As a result, the permeation rate of small molecules through the modified GO membranes was dramatically enhanced without sacrificing the selectivity.

Second, the oxygen-containing functional groups on GO flakes enable GO membranes to be chemically functionalized by inorganic nanoparticles, ions, organic compounds, polymers, etc.[44] Metal or metal oxide inorganic nanoparticles made of Pt, SiO_2, and TiO_2 can be added onto GO flakes as supporting materials using different chemical or physical approaches such as ultrasonic spray pyrolysis,[108] self-assembly,[109] and impregnation process.[110] Park *et al.* modified GO membranes with Mg^{2+} and Ca^{2+}, and Yeh *et al.* functionalized GO membranes with Al^{3+} by simply adding ion solution into GO solution during the membrane fabrication process.[42,43] The cations cross-linked the negatively charged functional groups on the GO flakes, and they held adjacent GO sheets together by ionic bonds. As a result, the mechanical strength of GO membranes was enhanced. GO can also be functionalized by organic compounds such as aromatic dyes,[111] and

pyrene by covalent or non-covalent approaches.[112] For the covalent approach, the oxygen-containing functional groups on GO flakes work as handles for the chemical modifications. With respect to the non-covalent approach, the strong adsorption of organic aromatic compounds onto GO flakes is attributed to π-π stacking.[113] Coleman *et al.* reported GO membranes functionalized by PEG molecules with three different molecular weights.[32] The polymers were grafted on to GO flakes using the carbodiimide chemistry. The stability of GO membranes in aqueous solutions was enhanced, and the permeation rate of ions through GO membranes was improved because the polymer chains enlarged the interlayer space within the modified membranes.

At last, a nanostrand-channeled GO membrane was reported by Huang and coworkers.[13] $Cu(OH)_2$ nanostands were mixed with GO solution to produce well-defined nanochannels within GO membranes with a narrow size distribution from 3 to 5 nm. After the GO solution was made into membranes, $Cu(OH)_2$ was easily removed by washing the membranes with acid solution. With the nanochannels left within the GO membranes, the modified GO membranes showed excellent mechanical strength and good separation performance in transport experiments. However, a reversible deformation of these nanochannels was observed when the modified GO membranes were operated under high pressure conditions, thus causing unstable permeation and rejection rates as a function of the pressure applied to the system.

Chapter 2. Ion and Solvent Transport through GO Membranes

2.1 Introduction

As introduced in the previous chapter, GO membranes have many great potential applications such as seawater desalination, alcohol dehydration, and water purification because of their unique properties and advantages. The mechanisms governing mass transport through GO membranes have been extensively discussed in recent years.[73-79] However, many mechanisms still remain debatable. Pressure-driven membrane processes are commonly used in various industrial applications, yet pressure-driven solvent transport through GO membranes has not been well-studied. In this work, GO was synthesized using a modified Hummers method and made into membranes via pressure filtration.

In order to investigate the mechanisms governing solvent transport through GO membranes, the pressure-driven permeation of water and water/ethanol mixtures through GO membranes were studied. In addition, the permeation of two charge equivalent and structurally similar ruthenium complex ions, tris(2,2-bipyridyl) dichlororuthenium(II) hexahydrate, $Ru(bpy)_3^{2+}$, and dichlorotris(1,10-phenanthroline)ruthenium(II) hydrate, $Ru(phen)_3^{2+}$, through GO membranes were studied as well.

2.2 Materials and Methods

GO was synthesized using a modified Hummers method.[49-50] First, graphite flakes (100 mesh, Sigma-Aldrich) were ground with sodium chloride and washed with deionized water. After drying, 3.0 g of ground graphite flakes were mixed with 1.5 g of sodium nitrate and 70 mL of 97% sulfuric acid (EMD) in a round-bottom flask. After stirring for 30 minutes, the mixture was then transferred to an ice bath, and 15.0 g of potassium permanganate ($KMnO_4$, EMD) was slowly added into the mixture while stirring. After $KMnO_4$ was added into the flask, the mixture was transferred to a 40 ℃ water bath and stirred for another two hours. Afterwards, the mixture was diluted with 140 mL of deionized water and heated to 95 ℃ while stirring. An hour later, 420 mL of deionized water and 20 mL of 30 wt% hydrogen peroxide were added into the mixture to stop the oxidation process while stirring. The suspension was then repeatedly centrifuged at 11,000 rpm for 12 minutes, followed by washing with 5% hydrochloric acid (HCl) twice and deionized water twice. The pellet was retained after each wash. After re-dispersing the precipitate into deionized water, ultra-sonication (30 min, Branson 2510) was applied to the mixture for 30 minutes to yield a suspension of single-layer GO, and then the solution was centrifuged again (10 minutes, 6 times, 3200 g) to remove the unreacted graphite particles. At last, the brown homogenous solution was dialyzed against Milli-Q water for seven days with water changed every day (molecular weight cut off MWCO 12000-14000 Dalton). The obtained golden-brown GO solution was collected and kept under ambient condition for future use. A thick GO membrane was made using 10 mL of the GO solution with the vacuum filtration method. By weighting the mass of this membrane, the concentration of the GO solution can be determined (normally ~ 5 mg/mL).

GO membranes were fabricated using pressure filtration of GO aqueous solutions.[11,71] A homemade pressure filtration device (Figure 2.1 a) was used for this purpose, which consisted of three main components. A gas inlet is located on the cap of this device and connected to

compressed nitrogen gas through a high precision regulator. A safety valve is located at the top of

the cap as well. The body of the device is a chamber that is used to contain solvents or solutions

(36 mm in diameter and 230 mm in length). The base of this device works as a bracket that supports

the polycarbonate filter membrane (40 mm diameter, 0.01 μm pore size, Whatman) and allows

filtrate to flow out through the liquid outlet at the bottom. The pressure filtration device is made

of stainless steel, and it can withstand pressure in the range of 0-40 psi. The stock GO solution

(Figure 2.1 b) was first diluted to 0.1 mg/mL. By adding a fixed volume of the diluted GO solution

into this filtration device, the mass of each GO membrane was controlled. This setup was also used

for pressure-driven solvent transport experiments. Water, ethanol, or mixtures of water and ethanol

with various molar ratios were added into the chamber of the device, which was then pressurized

to 5 to 30 psi above the atmosphere pressure. After each fixed time interval, mass and volume of

the filtrate were recorded to calculate the flux of solvent through GO membranes. Index refraction

(Appendix A) was used to determine the molar ratio of ethanol in water/ethanol mixtures. A

calibration curve was drawn to convert index refraction readings to ethanol molar percentage
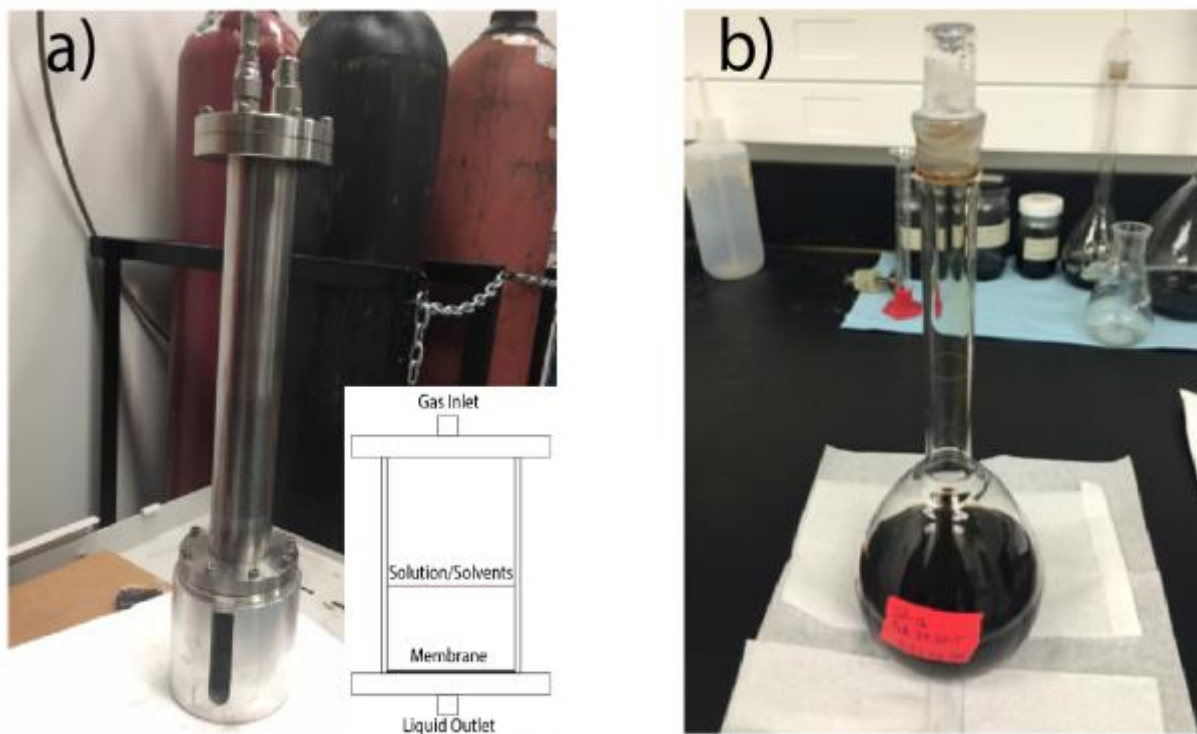
values.

Figure 2.1 GO and GO membrane. (a) An optical image and a schematic drawing of the homemade pressure filtration device. (b) An optical image of a GO aqueous solution.

Fourier transform infrared spectroscopy (Bruker Tensor 37 FTIR spectrometer), atomic force microscopy (AFM, Veeco Nanoscope Multimode AFM), scanning electron microscopy (SEM, LEO FE-SEM1530, Watlab), X-ray diffraction (XRD, Bruker D8-advance), and thermogravimetric analysis (TGA, TA instruments SDT Q600) were applied to characterize GO and GO membranes. FTIR was used to confirm the oxidation of graphene. The GO solution was freeze dried for 24 hours before each FTIR measurement. The dry GO powder was ground with KBr, and then compressed into a small tablet. Water had to be avoided in the whole process. AFM was operated in the tapping mode using a cantilever with resonance frequency at 280 kHz. To prepare samples for AFM, the GO solution was diluted to approximately 0.01 mg/mL, then

20

deposited on freshly cleaved mica (Ted Pella). SEM was operated in the secondary electron mode with an accelerating voltage set at 5 kV. GO membranes were stuck on stubs using carbon tape, and coated with gold to avoid electron accumulation. XRD experiments were performed on a diffractometer equipped with Cu K_α radiation at 1.542 Å. The scanning angle (2θ) was from 5° to 20°. For TGA, the temperature was increased from 25 to 1000 ℃ with a ramp rate of 10 ℃/min. Solid GO was freeze dried for at least one day in advance, then loaded into an alumina crucible. The air flow was set at 100 mL/min.

The experimental setup for ion transport experiments is shown in Figure 2.2. For protection, GO membranes were placed in the middle, fully covered by two pieces of polycarbonate filter membranes, and then sandwiched by two PDMS O-rings (diameter = 4 mm, area = 12.6 mm^2). Two polystyrene cuvettes were used as the feed and the permeate reservoirs. The cuvettes, PDMS o-rings, filter membranes, and GO membranes were clamped together. Before each transport experiment, both the two cuvettes were filled up with deionized water to ensure that the GO membranes were fully hydrated. To start an ion transport experiment, the water in the 'feed' reservoir was replaced with 2 mL of 20 mM Ru(bpy)$_3^{2+}$ or Ru(phen)$_3^{2+}$ ion aqueous solution, and the permeate reservoir was filled up with 2 mL of Milli-Q water to ensure that no liquid pressure difference existed between the two cuvettes. During the experiment, 0.1 mL of liquid was collected from the permeate cuvette at different time points, and then diluted with 0.9 mL of Milli-Q water. UV-Vis absorption (PerkinElmer Lambda 25) of the diluted samples was measured afterwards. At the same time, 0.1 mL of ion aqueous solution would be taken from the 'feed' cuvette to keep the heights of the solutions on both sides at a same level. The optical absorption maxima of Ru(bpy)$_3^{2+}$ and Ru(phen)$_3^{2+}$ ions are located at 450 nm and 448 nm respectively.
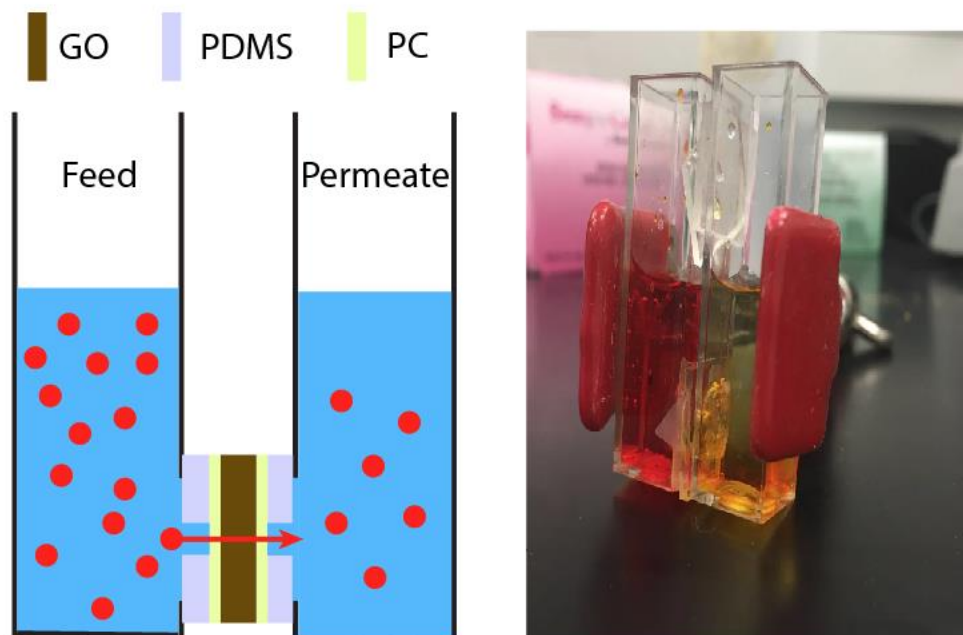
Figure 2.2 Ion transport measurement setup. A schematic drawing (left) and an optical image of the ion transport measurement setup.

2.3 Results and Discussion

2.3.1 GO and GO membrane characterizations

As shown in Figure 2.3, the FTIR spectrum for GO was obtained from 4000 cm^{-1} to 600 cm^{-1}. The labeled peaks are attributed to C-O-C epoxide stretching (1080 cm^{-1}), C-OH stretching (1250 cm^{-1}), O-H bending vibration (1385 cm^{-1}), C=C stretching (1630 cm^{-1}), C=O stretching (1730 cm^{-1}), C-H alkane stretching (2918 cm^{-1} and 2858 cm^{-1}), and O-H stretching (3430 cm^{-1}).[53-56] The large O-H peak at 3430 cm^{-1} is mainly from water molecules absorbed from air.
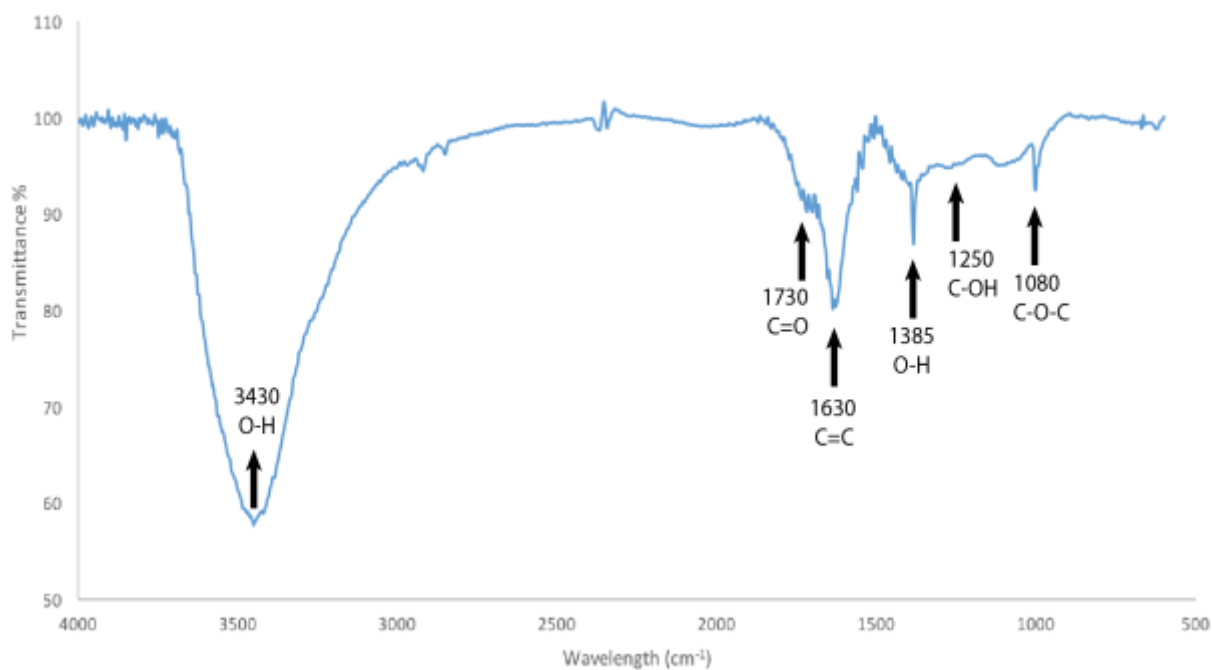

Figure 2.3 FTIR spectrum of GO.

Figure 2.4a shows an AFM image of GO sheets. The cross-sectional analysis of the AFM image shows that the thickness of the single layer GO flake is 0.8 nm which matches the values mentioned in previous reports (~1 nm).[51-52] As shown in Figure 2.4b, the interlayer space within dry GO membranes is determined to be 0.7 nm from the XRD spectrum. Figure 2.4c shows a cross-sectional SEM image of a GO membrane. The stacked-layers structure is obvious in this image, and the thickness of this 1.0 mg/cm^2 GO membrane is determined to be 5.2 μm.
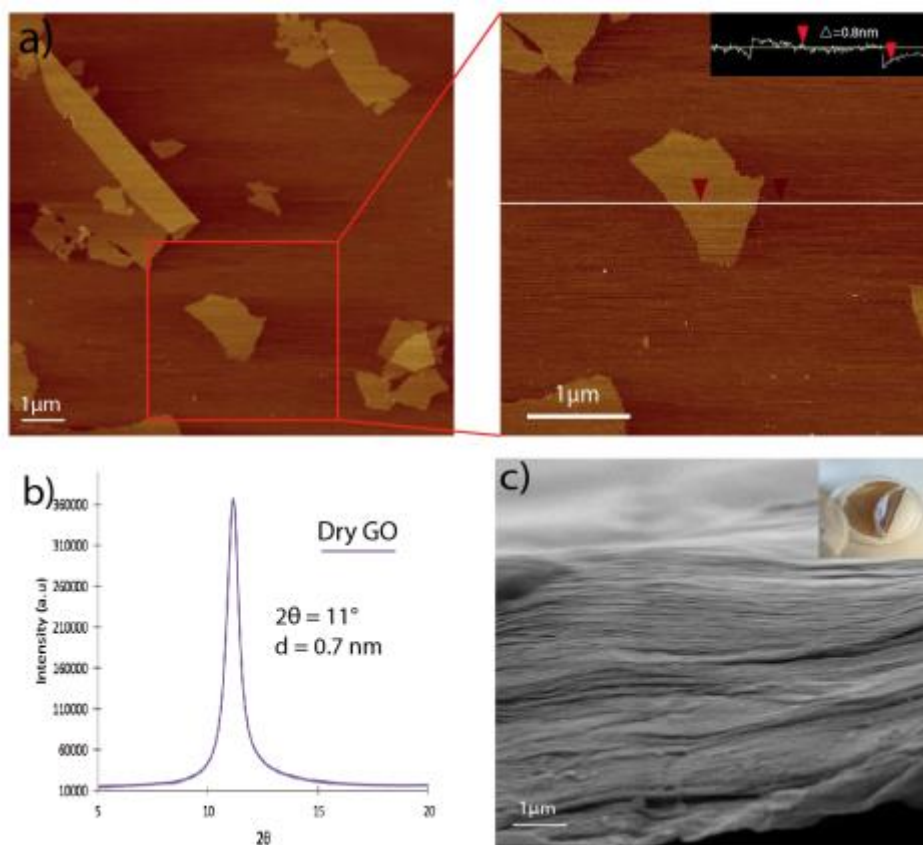

Figure 2.4 GO and GO membrane characteristics. (a) An AFM image of GO flakes with a cross-sectional analysis (inset). (b) XRD spectrum of a dry GO membrane. (c) Cross-sectional SEM image of a 1.0 mg/cm^2 GO membrane. Inset: an optical image of a whole GO membrane 3.6 cm in diameter.

2.3.2 Pressure-driven solvent transport through GO membranes

The pressure-driven solvent transport through GO membranes was studied using the method that was mentioned in the previous section. The pressure due to the solvent itself in the chamber is ~0.2 psi which is negligible (less than 5% compared to the gas pressure). Therefore, the predominate driving force of solvent transport was the pressure provided by compressed nitrogen gas. The thickness of GO membranes was kept constant at 5.2 μm and the mass density was kept at 1.0 mg/cm^2. The flux (J) of water and water/ethanol mixtures were calculated and plotted in Figure 2.6, and the rejection rate of ethanol from the ethanol/water mixtures was recorded in Table 2.1.

As shown in Figure 2.6a, the flux of water through GO membranes is proportional to the pressure applied to the system from 0 to 30 psi. The permeance of water through the GO membranes, i.e. the slope of the fitted line, was calculated to be 0.01 mL/h·psi·cm^2 which agrees with the permeance of water through GO membranes reported in a previous study.[13]

For the transport of water/ethanol mixtures through GO membranes under pressurized conditions (30 psi), the total volumetric flux was plotted as a function of ethanol molar percentage in Figure 2.6b. When the ethanol molar percentage in the binary mixture increased from 0% to 25%, the flux of the solvent mixture decreased dramatically. The lowest flux of the binary solvent mixture through GO membranes was observed at 25% ethanol. When the ethanol molar percentage in the mixture continued to increase from 25% to 100%, the flux of the water/ethanol mixture through the GO membrane increased again. Compare to the results reported previously in the literature (Figure 2.5a b), the transport phenomenon of GO membranes showed high similarity to the transport of water/ethanol mixture through semi-hydrophilic and hydrophilic membranes. Being different from the hydrophilic membranes, the flux of water/ethanol solvent mixture through

hydrophobic membranes shows high dependence on polarity of the solvent mixtures (Figure 2.5c).[69] Since GO membranes are semi-hydrophilic by nature, this observation suggests that the hydrophilicity dominates on GO are important to solvent transport.

Because of the reduced membrane-solvent interaction, polar solvents can easily travel through hydrophilic membranes. It is known that water has greater polarity than ethanol. Adding ethanol into water causes the polarity of water/ethanol mixtures to continuously decrease. Therefore, if polarity of the solvent mixtures is the main factor that governs the permeation of water/ethanol mixtures through the hydrophilic GO membrane, the flux of the solvent mixtures through membranes should decrease continuously until the molar percentage of ethanol reaches 100%. However, a minimum was found at 25% ethanol in Figure 2.5b which suggests that the viscosity of the solvent mixtures dominates the flux of the water/ethanol through GO membranes because the viscosity of a water/ethanol mixture reaches its peak value at 25% ethanol. Increasing or decreasing of the ethanol molar percentage causes viscosity of the mixture to decrease. To confirm the relationship between the viscosity and the flux of the solvent mixtures through the GO membranes, the flux was plotted as a function of the inverse of viscosity in Figure 2.6c.[72] As expected, a linear relationship was observed between the flux and the inversed viscosity of mixtures. Therefore, we conclude that viscosity dominates the permeance of the solvent mixture through GO membranes, and polarity of the water/ethanol mixture can also affect the total volumetric flux of the binary mixture through GO membranes.
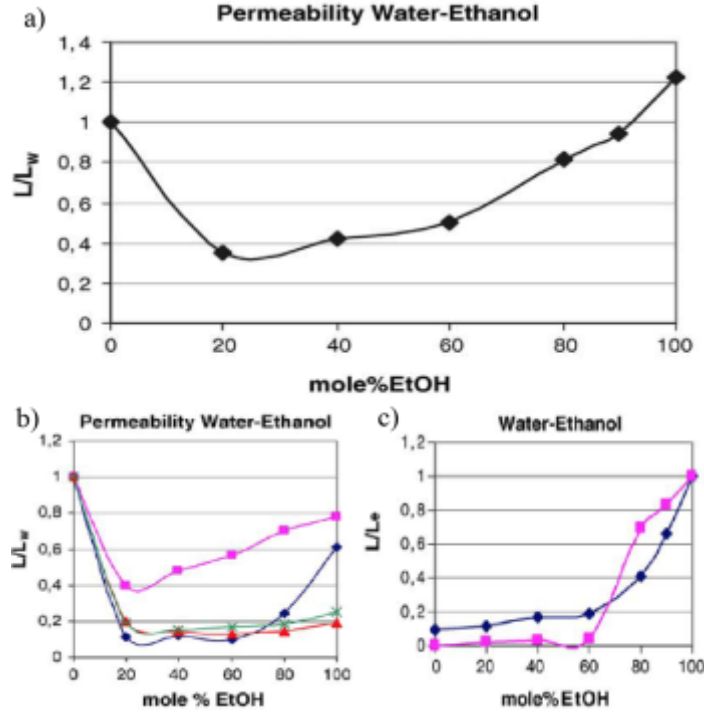
Figure 2.5 Normalized permeability of water/ethanol mixtures through membranes as a function of molar percentage of ethanol. (a) Semi-hydrophilic membrane. (b) Hydrophilic membranes. (c) Hydrophobic membranes. Reprinted with permission from Ref. 69.

Based on the discussion of the permeation of hydrated ion through GO membranes reported in a previous study, the viscous flow of water/ethanol mixture through thick GO membranes is assumed to be dominated by the slit pores mentioned in the previous chapter. As a result, a modified HP equation was applied here to approximately estimate the volumetric flux of solvent through GO membranes,

$$J = \frac{h^4 \Delta P}{12 \eta L^2 \Delta x} \tag{2.1}$$

where J is the flux of ethanol/water mixture, h is the channel size (interlayer space ~ 1 nm determined by XRD) inside the hydrated GO membranes, ΔP is the pressure applied to the system (30 psi), η is the viscosity of the solvent (889 μPa·s for water), L is the lateral length of GO flakes (220 nm determined by dynamic light scattering under the assumption that GO flakes behave as spheres), and Δx is the thickness of GO membranes (5.2 μm determined by SEM).

Equation 2.1 yields a flux of 0.03 mL/h·cm^2 at 30 psi for pure water permeation through GO membranes. However, we found experimentally the flux equaled 0.28 mL/h·cm^2 which is around ten times greater than the calculated value. The capillary force and frictionless water flow in the nanochannels in the GO membranes could be the reasons for this faster water transport. Another reason could be the disorder of the GO membrane after hydration.
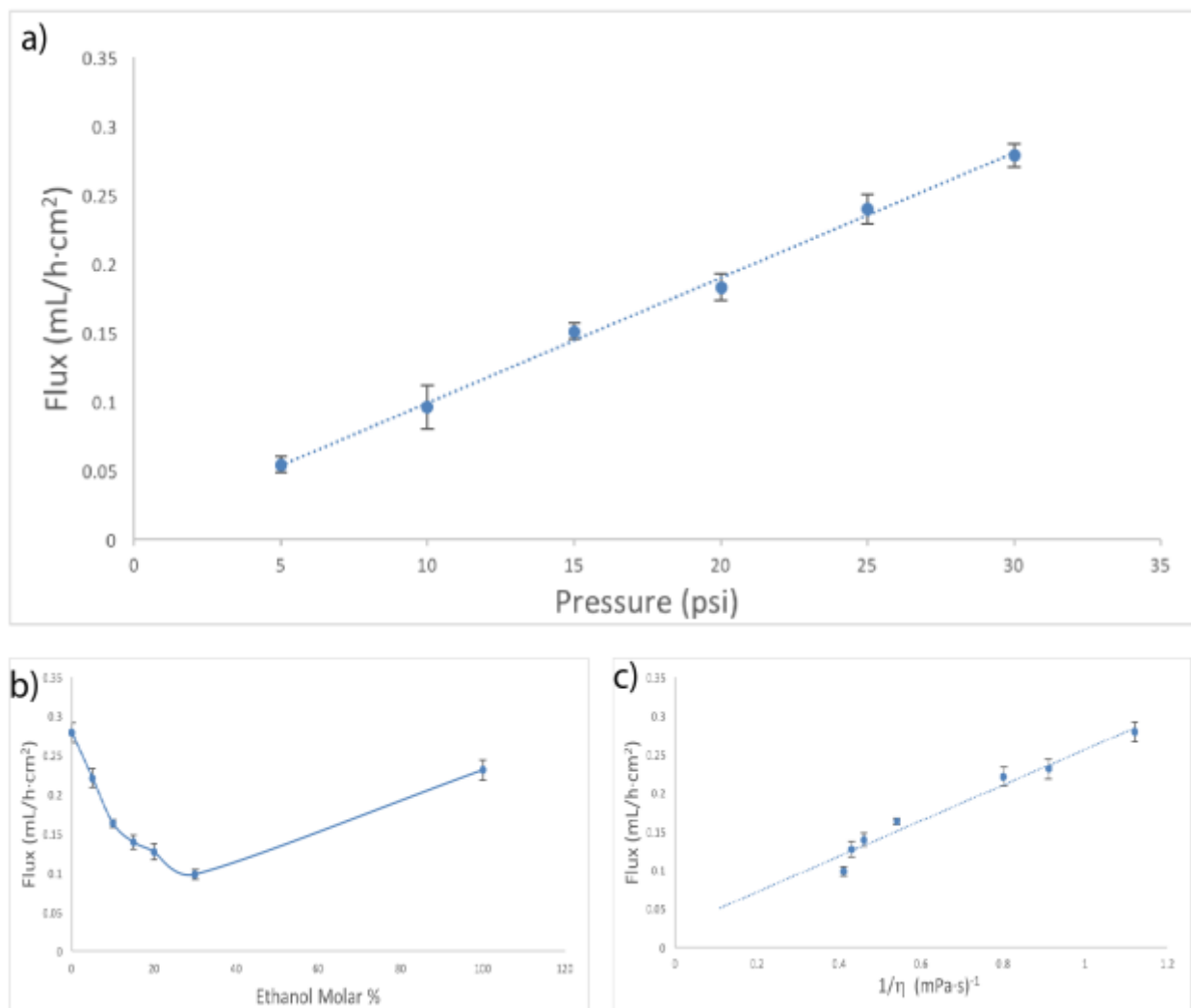
Figure 2.6 Pressure-driven solvent transport through GO membranes. (a) Flux of water as a function of pressure. (b) Flux of ethanol/water as a function of ethanol mole %. (c) Flux of ethanol/water mixtures as a function of viscosity, under a constant pressure of 30 psi.

The rejection rates of ethanol from the binary water/ethanol mixtures were measured and recorded in Table 2.1. Due to the limitation of our method, only mixtures with 0-30% ethanol were studied. The partial permeability of water/ethanol binary mixture through GO membranes was calculated and plotted in Figure 2.7a. The volumetric flux of 100% ethanol through GO

29

membranes was recorded as 0.23 mL/h·cm^2 which was not labeled in the figure. The ethanol molar percentage of the filtrate was also plotted in Figure 2.7a. It is obvious that the molar percentage of ethanol in the binary solvent mixture was decreased after filtering through the GO membranes. Ethanol molecules can form clusters in water/ethanol mixtures. The hydrated ethanol clusters usually have more than eight ethanol molecules.[115] The radius of these clusters is larger than 1 nm which is approximately greater than the size of the nanopores in GO membranes.[116] Therefore, the energy barrier that is caused by the decomposition of ethanol clusters becomes one of the main reasons for the decreased ethanol concentration in the filtrates. Besides the steric hindrance effect, interactions between the membrane surface and solvent molecules are also affacting the rejection of ethanol through GO membranes. Compared to the results reported previously in the literature, the transport phenomenon of GO membranes showed high similarity to the transport of water/ethanol solvent mixtures through semi-hydrophilic membranes as shown in Figure 2.7b, but it was very different from the transport of water/ethanol solvent mixtures through hydrophobic membranes as shown in Figure 2.7c.[69] This observation confirms the hydrophilic nature of GO membranes. It also suggests that the polarity of solvents and the hydrophilicity dominates on GO membranes are important to the rejection rates of ethanol from water/ethanol mixtures as well. Because of the reduced repulsion and resistance between solvent molecules and membrane surfaces, polar solvent molecules can travel through hydrophilic membranes faster than non-polar solvent molecules. Since water has greater polarity than ethanol, GO membranes reject ethanol molecules, thus resulting in the decreased ethanol concentration in the filtrates.

Ethanol molar percentage in original mixtures (%)	Ethanol molar percentage in filtrate (%)
5.0	1.3 ± 0.1
10.0	2.6 ± 0.3
15.0	2.5 ± 0.2
20.0	9.3 ± 0.2
30.0	14.2 ± 1.0

Table 2.1 Selectivity of GO membranes for ethanol/water mixtures under a constant pressure of 30 psi.

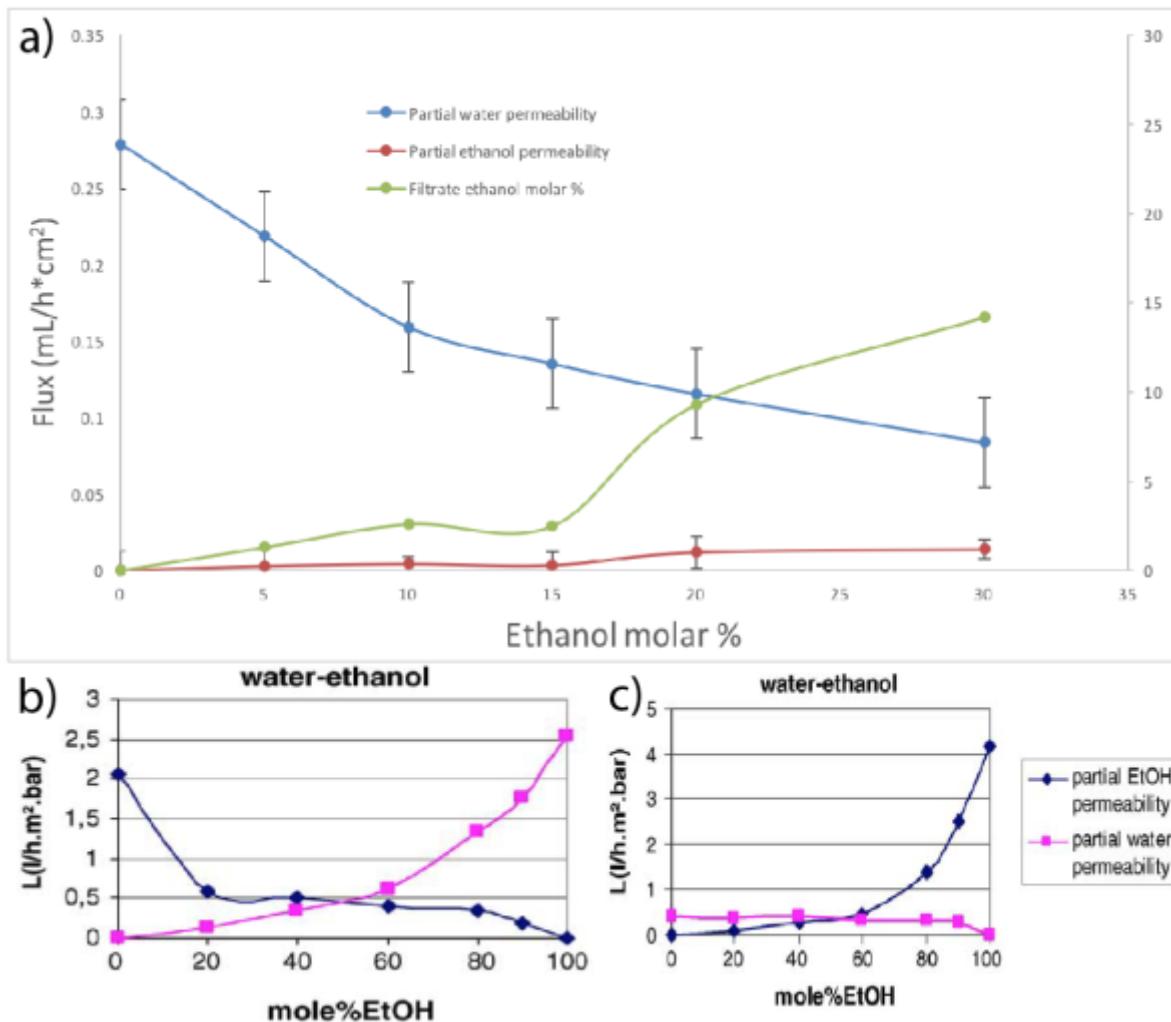**Figure 2.7** Partial permeability of water/ethanol mixtures through membranes. (a) Flux of solvent mixtures through GO membranes as a function of ethanol molar %. (b) Normalized flux of solvent mixtures through semi-hydrophilic membranes as a function of ethanol molar %. (c) Normalized flux of solvent mixtures through hydrophobic membranes as a function of ethanol molar %. Reprinted with permission from Ref. 69.

2.3.3 Ion Diffusion through GO Membranes

Ion diffusion through 1.0 mg/cm^2 GO membranes was also studied in this work. The ion concentration of the solutions was measured by ultraviolet-visible spectroscopy (UV-vis), and the moles of Ru(bpy)$_3^{2+}$ and Ru(phen)$_3^{2+}$ ions that permeated through the GO membranes in six hours were calculated and plotted in Figure 2.8. Permeance of the two ruthenium complex ions through our 5.2 μm GO membranes was observed in this work contrast to what was observed by Joshi et al.[25,30] A possible explanation for this contrast is that the GO flakes used in this test had an average lateral size ~220 nm which is much smaller than the size of GO flakes (1 μm) reported by Joshi and coworkers. The GO flakes with a smaller size are able to build up nanoporous structures with higher porosity in the GO membranes, thus affecting the rejection rate of the GO membranes.

Because the active area of GO membranes (12.6 mm^2) is already known, the fluxes of the two complex ions through GO membranes were then calculated as 1.55 mmol/hr·m^2 for Ru(bpy)$_3^{2+}$ and 0.67 mmol/hr·m^2 for Ru(phen)$_3^{2+}$, which agree with the flux values reported by Coleman *et al.*[32]
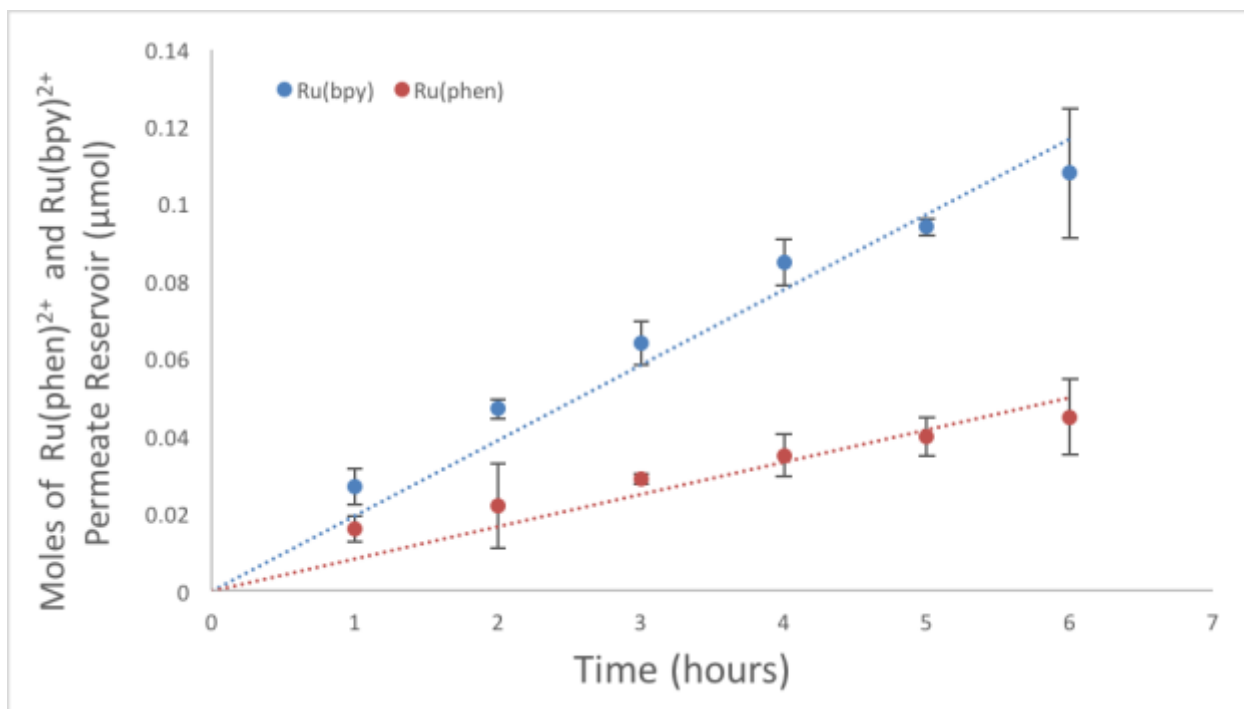
Figure 2.8 Concentration driven permeation of $Ru(phen)_3^{2+}$ and $Ru(bpy)_3^{2+}$ ions through GO membranes.

Based on the Equation 1.4, 1.5 and 1.6 mentioned in the Chapter 1.

$$\text{MFR} = D\Delta C \frac{A_e}{L_e} \tag{1.4}$$

$$A_e = A \cdot \frac{d}{L} \tag{1.5}$$

$$L_e = L \cdot \frac{h}{d} \tag{1.6}$$

The effective area of the GO membranes was calculated as

$$12.6 \text{ mm}^2 \text{ x } \frac{1 \, nm}{220 nm} = 0.048 \text{ mm}^2$$

The effective length of the GO membranes was calculated as

$$220 \text{ nm} \times \frac{5.2 \, \mu m}{1 \, nm} = 1.64 \text{ mm}$$

The bulk diffusivities of $Ru(bpy)_3^{2+}$ and $Ru(phen)_3^{2+}$ ions were calculated by the Stokes-Einstein equations as 3.87×10^{-10} m^2/s for $Ru(bpy)_3^{2+}$ and 3.70×10^{-10} m^2/s for $Ru(phen)_3^{2+}$.[32] With the ΔC equals to 20 mM, the theoretical permeation rates of $Ru(bpy)_3^{2+}$ and $Ru(phen)_3^{2+}$ ions through GO membranes were calculated as 0.144 ng/s and 0.139 ng/s. However, being different from the ultrafast ion permeation reported by the previous studies, the experimental permeation rates of the complex ions were only 5-10 times greater than the theoretical values. A possible explanation is that the frictionless aqueous ion solution flow in the nanochannels may not be suitable for describing the diffusion of large hydrated ions through GO membranes.

The flux ratio of these two complex ions through GO membranes (J_{phen}/J_{bpy}) was also calculated as 0.44. Since the two ions are charge equivalent, structurally similar, and traveling through the same nanochannels within GO membranes, the significant permeance difference cannot be explained by capillary force, electrostatic force, or π-π interaction.[98] The only difference that could cause the contrast of flux between these two ions is their size difference which is at sub-angstrom scale. Therefore, GO membranes are proven to be highly sensitive to the small difference of the ion size.

2.4 Conclusion

In summary, GO was synthesized, and the GO solution was used to prepare GO membranes using a homemade pressure filtration device. Pressure driven water and water/ethanol mixture transport through 5.2 μm thick GO membranes were investigated in this study. The permeation rates of the solvents through the GO membranes were proportional to the pressure applied to the system and the inversed viscosity of the solvent mixture. The HP equation was applied to estimate the theoretical permeation rates of solvents through the GO membranes, but the experimental result was ~10 times greater than the theoretical value. The capillary force, frictionless water flow within the nanochannels, and the disorder of the GO membrane after hydration were considered as the main reasons for this phenomenon. The steric hindrance effect and solvent-membrane interaction were the main influence of the rejection of ethanol from water/ethanol mixtures through GO membranes.

Diffusive transport of two charge equivalent and structurally similar ruthenium complex ions, namely $Ru(bpy)_3^{2+}$ and $Ru(phen)_3^{2+}$, through GO membranes was also studied in this chapter. The experimental fluxes of the complex ions through the GO membranes were only a few times greater than the theoretical value predicted by Fick's first law. The flux ratio of the two complex ions was also calculated as $J_{phen}/J_{bpy} = 0.44$. The steric hindrance effect was confirmed as the main reason for the significant permeance difference between $Ru(bpy)_3^{2+}$ and $Ru(phen)_3^{2+}$ ions.

Chapter 3. Ion and Solvent Transport through Functionalized GO Membranes

3.1 Introduction

As mentioned in Chapter 1, functionalization of GO membranes can improve the stability and the separation performance of GO membranes. Various methods for functionalization of GO membranes have been explored in recent years.[99-100] For instance, the epoxy groups and the carboxyl acid groups on GO flakes can react with amine groups by ring-opening reactions or condensation reactions to graft amine-terminated polymers onto the GO surfaces.[101-102]

In this work, two methods were applied to create functionalized GO membranes. First, GO was functionalized with amine-terminated PEG by carbodiimide chemistry. Second, aluminum ions were intercalated into GO membranes by simply pressurizing aluminum chloride solution through GO membranes. Various characterization techniques, including TGA, SEM, and AFM were used to analyze the PEGylated-graphene oxide (PEG-GO) membranes and aluminum ion intercalated graphene oxide (Al-GO) membranes. Ion diffusion and pressure-driven solvent transport through PEG-GO and Al-GO membranes were investigated using the same methods and setup described in Chapter 2.

3.2 Materials and Methods

The Al-GO membranes were fabricated using the same pressure filtration device mentioned in the previous chapters. First, a 1.0 mg/cm^2 GO membrane was fabricated and dried in the pressure filtration device. Second, 20 mL of 1 M aluminum chloride ion solution was filtered through the GO membrane under a pressure of 30 psi. At last, the Al-GO membrane was washed with water by filtering 50 mL of deionized water through the Al-GO membrane three times to remove excess and loosely bonded aluminum ions within the Al-GO membrane.

To create PEG-GO membranes, GO was first reacted with the amine-terminated linear PEG using carbodiimide chemistry.[103] First, 25 mg of GO was added into 36 mL of 2-(N-morpholino) ethanesulfonic acid (MES) buffer solution (pH = 4.5) with 50 mg PEG (M_w = 6000), as well as 1-ethyl-3-(3-dimethylaminopropyl) carbodiimide (EDC, GBiosciences) and N-hydroxysuccinimide (NHS, Alfa Aesar) in excess. The mixture was stirred at room temperature for 24 hours and then was dialyzed against Mili-Q water for three more days with water changes twice a day (MWCO12000-14000 Da.). After that, the PEG-GO solution was collected and stored for future use. The PEG-GO membranes were fabricated with the same method that was used to make the GO membranes. The mass of GO within each PEG-GO membranes was kept constant at 10 mg.

AFM (Veeco Nanoscope Multimode AFM), SEM (LEO FE-SEM Watlab), XRD (Bruker D8-advance), TGA (TA instruments SDT Q600) were applied to characterize the functionalized GO and functionalized GO membranes. The methods and operations are identical to the protocol outlined in Chapter 2.

3.3 Results and Discussion

3.3.1 Functionalized GO membrane characterizations

FTIR was used to verify the functionalization of GO. The FTIR spectrum of PEG-GO is shown in Figure 3.1. Compared to the FTIR spectrum of GO, additional peaks are present at 950 and 840 cm^{-1} attributed to the rocking of the C-H groups, 1460 and 1352 cm^{-1} attributed to the bending of the C-H groups, 1100 - 1640 cm^{-1} for N-H and C-N vibrations, and 2938 cm^{-1} for C–H stretching.
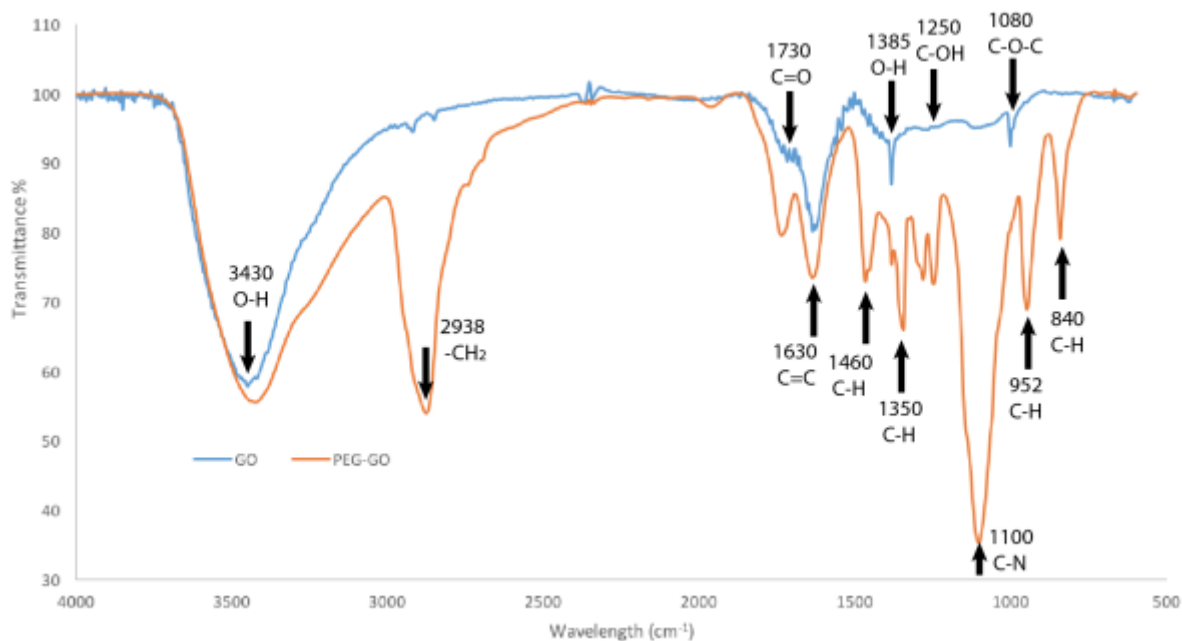

Figure 3.1 FTIR spectrum of PEG-GO.

Figure 3.2b shows an AFM image of individual PEG-GO sheets. Compare to the AFM image of GO flakes (Figure 2.4a), the polymer appears on individual GO sheets. Besides the FTIR

spectrum of PEG-GO described above, this AFM image evidently confirms that linear PEG was successfully grafted onto the surface of the GO sheets. Figure 3.2a shows a cross-sectional SEM image of a PEG-GO membrane. The stacked-layer structure is obvious in this image. Since the mass of GO in each PEG-GO membrane is the same as that in a pure GO membrane (10 mg, 1.0 mg/cm^2), the total mass of a PEG-GO membrane is greater than a pure GO membrane, and the thickness of PEG-GO membranes (6.4 μm) is greater than GO membranes (5.2 μm) as well. Figure 3.2c shows the TGA curve of the PEG-GO membrane. Since the thermal decomposition of different components in the PEG-GO membrane happens in different temperature ranges, trend lines (dashed lines shown in Figure 3.2c) of each linear part in this TGA curve were drawn to find the intersections, and then, the whole curve was divided into four sections which are shown as the shaded areas in Figure 3.2c. From 0 to 172 ℃, the first part of the weight loss is caused by the evaporation of water molecules that are adsorbed on the membrane. From 172 to 294 ℃, the thermal decomposition of the oxygen-containing functional groups is the main reason for the weight loss. From 294 to 345 ℃, the significant loss of mass is caused by the thermal decomposition of the PEG polymer chains. At last, from 345 to 500 ℃, the carbon network of GO decomposes. Based on this analysis, the mass composition of PEG-GO membranes is determined as: 7.7% water, 43.7% PEG polymer, and 48.6% GO.
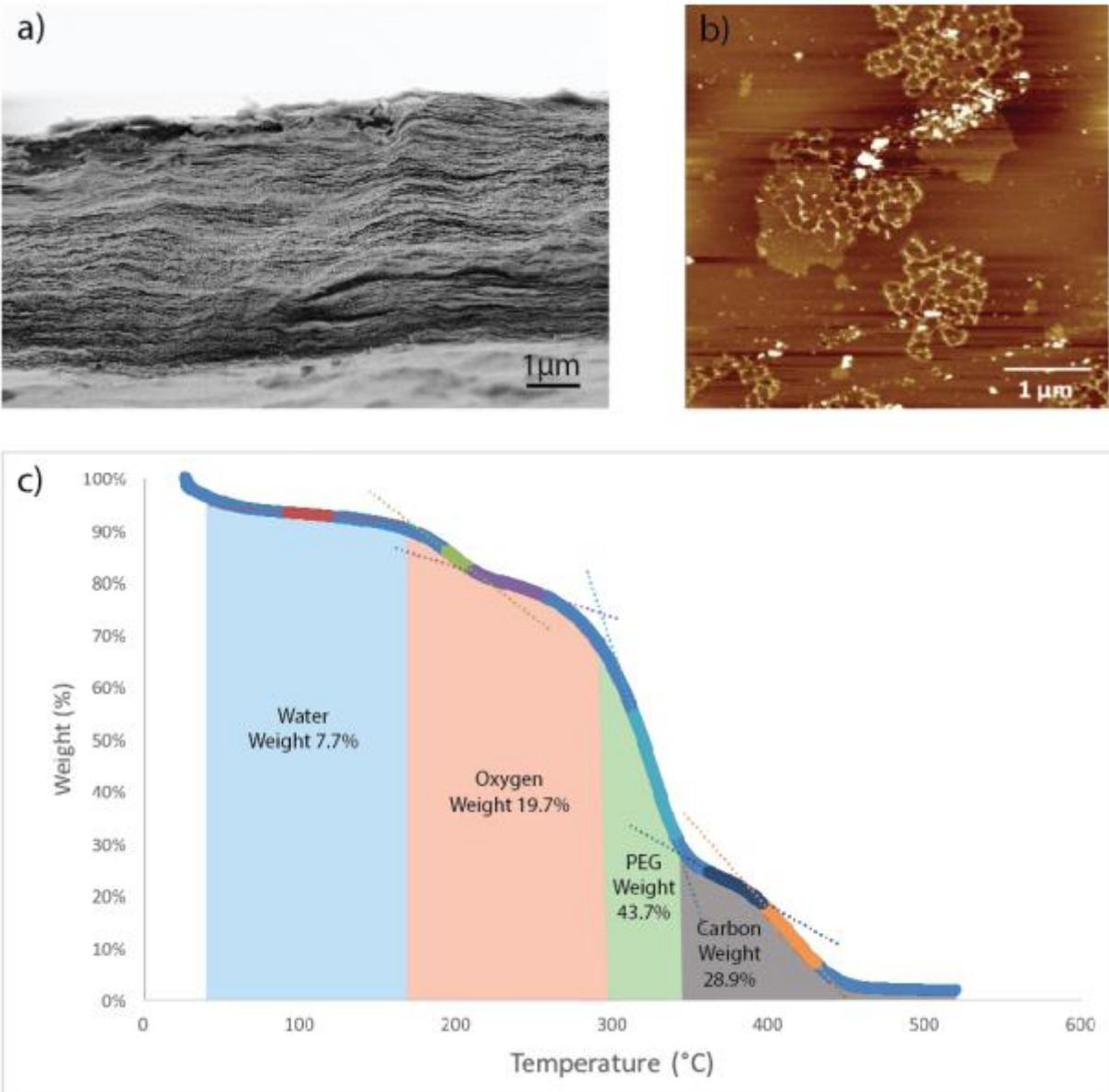
Figure 3.2 PEG-GO membrane characteristics. (a) A cross-sectional SEM image of PEG-GO membrane. (b) An AFM image of PEG-GO platelets. Reprinted with permission from Ref. 32 (c) TGA curve of PEG-GO.

The XRD spectrum of a dry PEG-GO membrane is shown in Figure 3.3a. Compared to the XRD spectrum of GO membranes (Figure 3.3b), the peak shifts to the left from 11° to 7.4°. This indicates that the interlayer spacing expanded from 0.7 to 1.2 nm. Consequently, the porosity of the GO membranes being defined in the HP equation as h/L, where h is the interlayer space and L is the average lateral length of GO flakes, is greatly enlarged. In addition, the broadness of the peak shown in Figure 3.3 also indicates that the inner structure of the PEG-GO membrane is less ordered. Therefore, we conclude that grafting PEG polymers onto GO flakes may open up some closed nanopores between the individual GO flakes of the membranes. The formation of these nanopores can shorten the net length of the path that particles have to travel through in the GO membranes, thus resulting in a faster permeation.[11,32]
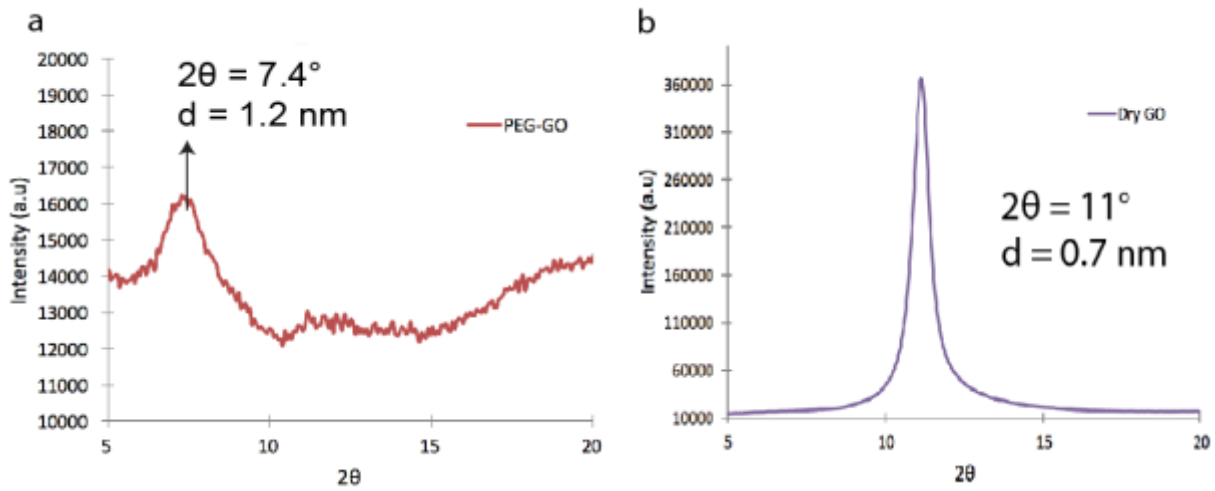

Figure 3.3 XRD spectra of (a) PEG-GO and (b) GO membranes.

3.3.2 Pressure-driven Solvent Transport through Functionalized GO Membranes

Because of the hydrophilic oxygen-containing functional groups, GO has excellent aqueous solution processability and solubility. However, this property of GO makes GO membranes easy to disperse in water by breaking the hydrogen bonds between adjacent GO sheets.[43] Functionalization of GO membranes helps to solve this problem. The covalent or ionic bonds between GO layers make functionalized GO membranes much more stable in aqueous solution.

The results of pressure-driven water transport through GO, PEG-GO, and Al-GO membranes are shown in Figure 3.4a. PEG-GO membranes have the greatest flux that is ~100% higher than GO membranes. Al-GO membranes have a greater flux than GO membranes as well. The shortened pathway, the expansion of the nanochannels, and the enlarged porosity within the GO membranes are the main reasons for this faster water permeation. However, different from what observed on GO membranes, the water flux through PEG-GO and Al-GO membranes was not completely proportional to the pressure applied to the system. Turning points were found between 15 psi and 20 psi for both PEG-GO and Al-GO membranes. The deformation of the nanochannels in the functionalized GO membranes under relatively high pressures is the main reason for this phenomenon because the compressed nanochannels would limit the water flow through the membranes.

The results of pressure-driven water/ethanol mixture transport through GO, PEG-GO, and Al-GO membranes are shown in Figure 3.4b and c. Similar to the GO membranes, the flux of this binary solvent mixture through the functionalized GO membranes is proportional to the inversed viscosity of the mixture. PEG-GO membranes have the greatest permeation rate. The Al-GO

membranes show lower solvent flux than PEG-GO membranes, but it is still greater than GO membranes. Since the transport results of the PEG-GO and Al-GO membranes are quite similar to the results obtained with the GO membranes, we conclude that the functionalization of the GO membranes with PEG and aluminum ions do not change the hydrophilicity of the GO membranes, and viscosity of the solvent mixtures remains the factor that dominates the total volumetric flux of the water/ethanol mixtures through the GO-based membranes.

The ethanol molar percentage of the filtrate was listed in Table 3.1, and the partial permeability of water/ethanol mixture through GO, PEG-GO, and Al-GO membranes was calculated and plotted in Figure 3.5. The results are similar to those reported water/ethanol mixture transport through semi-hydrophilic membranes in the literature. The partial permeation of water through these GO-based membranes decreased dramatically in the range of 0 to 30 molar percentage of ethanol, and the partial permeation of ethanol experienced a slow increase. This observation confirms that the hydrophilicity dominates on GO does not change after functionalization. The solvent-membrane interaction and the steric hindrance effect of ethanol clusters are still considered as the most important mechanisms that govern the rejection rate of ethanol through these GO-based membranes. Compared to GO membranes, Al-GO membranes have higher ethanol molar percentage in the filtrates. Because the aluminum ions can easily form ionic bonds with deprotonated functional groups on GO and make the edges of the GO flakes positively charged, the electrostatic force expands the nanochannels within GO membranes, resulting in the decreased rejection rate of ethanol through Al-GO membranes. Although the nanochannels within PEG-GO membranes are expanded as well, the grafted polymer chains reduce the interactions between the solvent molecules and the surface of PEG-GO. Therefore, the rejection rate of ethanol through PEG-GO membranes is only slightly lower than GO membranes.

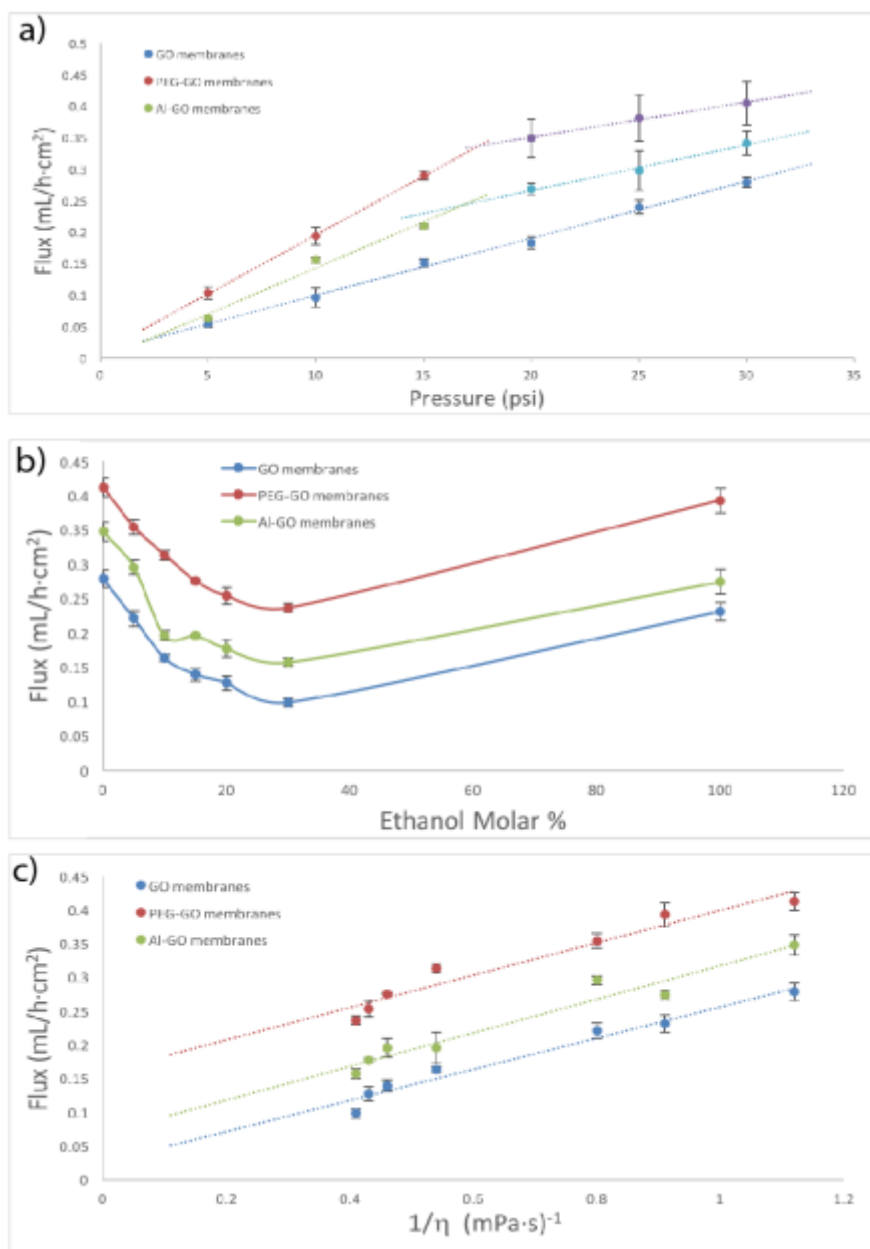**Figure 3.4** Pressure-driven solvent transport through GO-based membranes. (a) Fluxes of pressure-driven water transport through GO, PEG-GO, and Al-GO membranes as a function of pressure. (b & c) Pressure-driven ethanol/water mixture transport through GO, PEG-GO, and Al-GO membranes. (b) Plot of volumetric flux vs. ethanol mole %. (c) Plot of volumetric flux vs. viscosity, under a constant pressure of 30 psi.

Original Mixture	GO Membrane Filtrate	PEG-GO Membrane Filtrate	Al-GO Membrane Filtrate
5.0	1.3 ± 0.1	3.1 ± 0.2	1.4 ± 0.0
10.0	2.6 ± 0.3	5.0 ± 0.2	3.6 ± 0.2
15.0	2.5 ± 0.2	7.5 ± 0.3	5.1 ± 0.3
20.0	9.3 ± 0.2	10.0 ± 0.4	10.2 ± 0.2
30.0	14.2 ± 1.0	14.3 ± 0.1	17.2 ± 0.3

Table 3.1 Ethanol molar percentage (%) in the original ethanol/water mixtures and in the

filtrates after passing through GO, PEG-GO, and Al-GO membranes.
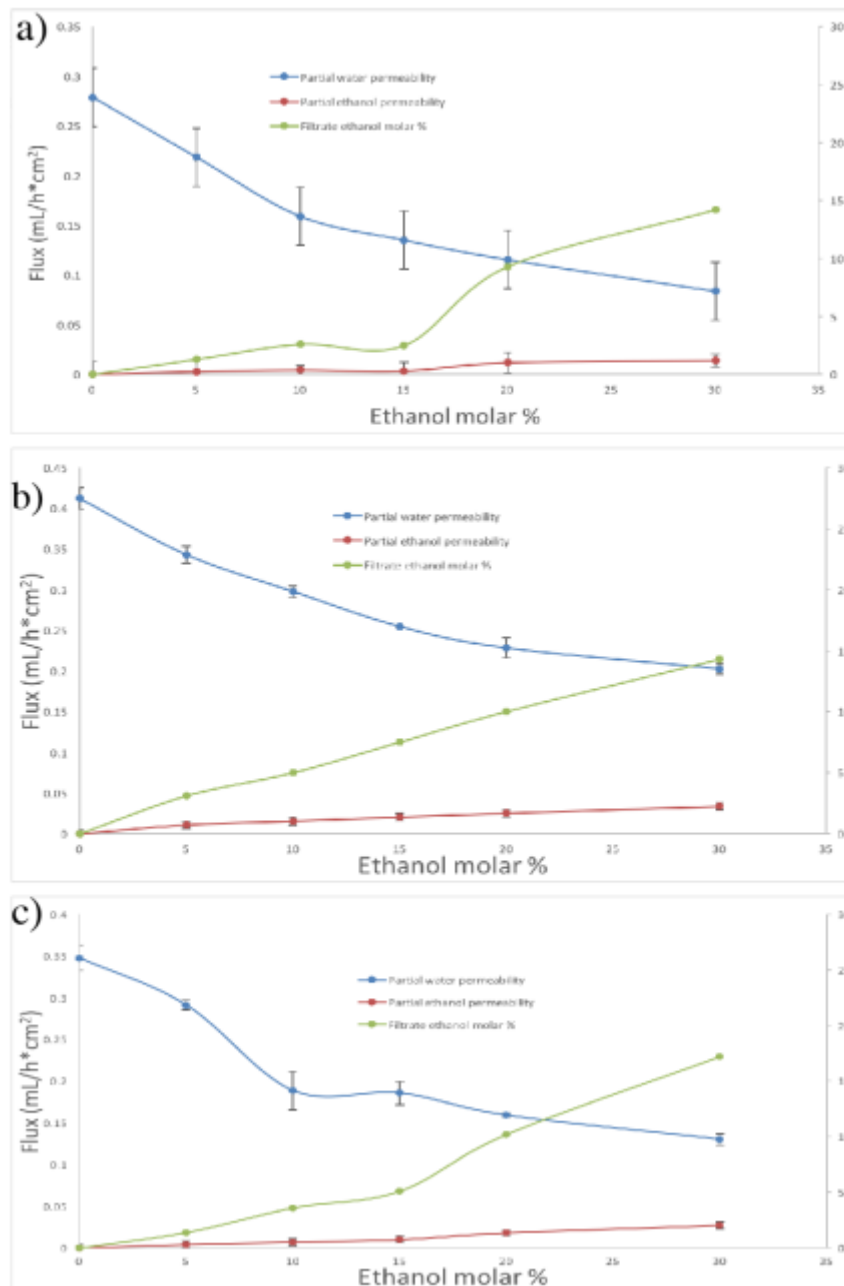
Figure 3.5 Partial permeability of water/ethanol mixture through membranes. (a) Flux of solvent mixtures through GO membranes as a function of ethanol molar %. (b) Flux of solvent mixtures through PEG-GO membranes as a function of ethanol molar %. (c) Flux of solvent mixtures through Al-GO membranes as a function of ethanol molar %.

3.3.3 Ion Diffusion through Functionalized GO Membranes

At last, the results of $Ru(phen)_3^{2+}$ ions transport through PEG-GO, Al-GO and GO membranes are shown in Figure 3.6. PEG-GO membranes show significantly greater (~300%) flux than pure GO membranes. The expansion of the channel size within PEG-GO membranes is the main reason for the faster ion permeation. In addition, the PEG polymer chains grafted onto GO flakes also reduce the possible interactions between the complex ions and the oxygen-containing functional groups on GO flakes, thus resulting in a much fluent flow of water and the complex ions.[104-106] On contrast, during the ion transport experiment, almost no flux of $Ru(phen)_3^{2+}$ and $Ru(bpy)_3^{2+}$ (Appendix B) ions through Al-GO membranes was observed in the first six hours. Based on the data obtained from a seven-days ion permeation test through Al-GO membranes, the fluxes of the complex ions through Al-GO membranes were determined to be 0.08 mmol/(hr·m^2) for $Ru(phen)_3^{2+}$ and 0.18 mmol/(hr·m^2) for $Ru(bpy)_3^{2+}$. The ion flux through GO membranes is around ten times greater than this value, and the ion flux through PEG-GO membranes is around thirty times greater than the ion flux through Al-GO membranes. The intercalated aluminum ions within the GO membranes are the reason for this phenomenon. Because the hydrophilic hydroxyl and carboxyl groups are normally located at the edges of the GO flakes, Al^{3+} ions can easily form ionic bonds with the deprotonated functional groups and block the nanopores between adjacent GO sheets to a certain extent, thus reducing the flux of large ions such as $Ru(phen)_3^{2+}$ and $Ru(bpy)_3^{2+}$ through Al-GO membranes. The electrostatic repulsion between the intercalated aluminum ions and the positively charged complex ions is another explanation for this slow permeation of ions through Al-GO membranes. However, because the aluminum ions are not covalently bonded to GO membranes, there is a possibility that the aluminum ions within Al-GO membranes can be replaced by the positively charged complex ions during the ion permeation

process. This mechanism needs to be further investigated by measuring the elementary composition in filtrates using energy-dispersive x-ray spectroscopy.
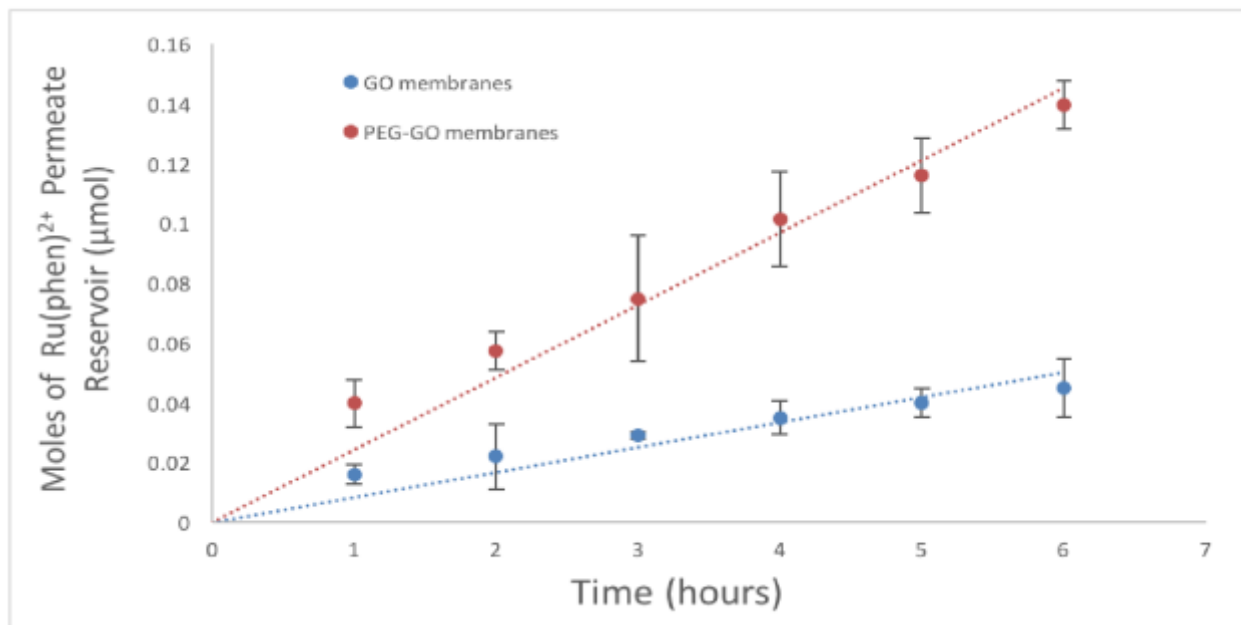

Figure 3.6 Concentration driven permeation of Ru(phen)$_3^{2+}$ ions through GO and PEG-GO membranes.

3.4 Conclusion

In this work, GO membranes were functionalized with PEG polymers and aluminum ions, and PEG-GO and Al-GO membranes were fabricated.

The pressure-driven solvent transport through PEG-GO and Al-GO membranes were investigated. Similar to GO membranes, the permeance of the solvents through PEG-GO and Al-GO membranes was proportional to the inversed viscosity of the solvent. The modified nanochannels within the functionalized GO membranes are easier to deform under pressure, thus reducing the permeation rate of solvent molecules through membranes above 15 psi. Because of the expanded nanochannels, the increased porosity, and the shortened pathway of transport, PEG-GO and Al-GO membranes show faster solvent permeation but lower rejection rate for ethanol than GO membranes.

Ion transport through functionalized GO membranes was also investigated. The expanded nanochannels in PEG-GO membranes and the reduced ion-membrane interactions are the main reasons for the faster ion permeation through PEG-GO membranes, while the blocked porous structure within Al-GO membranes and the electrostatic repulsion between intercalated aluminum ions and the positively charged complex ions are the main reasons for the extremely slow permeation rate of complex ions through Al-GO membranes.

Chapter 4. Summary and Future Work

4.1 Summary

GO shows great promise as a membrane material because of its unique properties such as strong mechanical strength, great flexibility, and large aspect ratio. In order to meet the urgent demand of the relevant industrial sectors, further research on GO-based membranes is needed in order to achieve high permeation rate and selectivity in various potential membrane applications. In this work, ion diffusion and pressure-driven solvent transport through GO and functionalized GO membranes have been studied.

GO was synthesized, and GO membranes were fabricated using the pressure filtration method. Water transport through GO membranes under various pressurized conditions and water/ethanol mixture transport though GO membranes under a pressure of 30 psi were studied to investigate the mechanisms governing the solvent transport through GO membranes. The results were presented in Chapter 2. The permeation rate of water through GO membranes was found to be proportional to the pressure applied to the system, and the experimental water flux was greater than the theoretical value calculated by the HP equation. The capillary force, frictionless water flow in the nanochannels, and the disorder of GO membranes after hydration might be the main reasons for the observed fast water permeation. The total volumetric flux of water/ethanol mixtures through GO membranes was inversely proportional to the viscosity of the solvent mixture. Preferential ethanol rejection was also observed. Our data suggests that steric hindrance and the interactions between the solvent molecules and the membrane surfaces dominate the rejection rate of ethanol through GO membranes. Transport of two charge equivalent and structurally similar

ruthenium complex ions through the GO membranes was also studied. With the steric hindrance effect in control of the ion selectivity of GO membranes, the molar flux of the ions through GO membranes was only a few times greater than the theoretical value calculated by Fick's First Law, which means the that enhanced ion permeation in aqueous solutions through GO membranes is not applicable to large complex ions.

In Chapter 3, studies on functionalized GO membranes were presented. GO membranes were functionalized either with amine-terminated PEGs polymers (PEG-GO) or aluminum ions (Al-GO). Due to the enlarged pore sizes, the permeation rates of solvents through both PEG-GO and Al-GO membranes are higher than those measured for the GO membranes, while the rejection rates for ethanol through both types of membranes were lower than that obtained with the GO membranes. Deformation of the nanochannels in the functionalized GO membranes happened when the membranes were operated under highly pressurized conditions, and consequently a reduced solvent permeation through membranes was observed. Ion transport through the PEG-GO and Al-GO membranes was also studied. Compared to the GO membranes, the expansion of the nanochannels in the PEG-GO membranes and the reduced ion-membrane interactions resulted in faster ion transfer. In contrast, slower ion permeation through Al-GO membranes was observed. The blocked nanopores and the electrostatic repulsion between the intercalated Al^{3+} and the solute ions are likely the reasons. The intercalated aluminum ions can be replaced by other positively charged ions during the ion permeation process.

4.2 Future Work

GO membranes have many potential applications in the future. Building on this work where water, water/ethanol mixtures and ruthenium complex ion transport through GO-based membranes were studied, experimental setup could be further improved in the future.

First, in this work, deformation of nanochannels was observed to affect the permeance of the solvent through the functionalized GO membranes. A new pressure filtration device could be designed to carry out more systematic studies on the pressure dependence of solvent permeation and rejection rates through the functionalized GO membranes. Second, to avoid any large crack on the GO-based membranes affecting the experimental results, a gas-leakage detection system can be designed to test the integrity of the GO-based membranes before they are subjected to the transport experiments. Third, for the study of solvent transport through the GO-based membranes, measurements of the membranes' contact angle and the polarity of solvent mixtures would help to clarify the effects of solvent-solvent and solvent-surface interactions in the GO-based membranes.

For future projects, can electric potential can be applied as the driving force for mass transport through the GO-based membranes, besides chemical potential and pressure. Electrophoresis and electro-osmosis experiments can be carried out on the GO-based membranes. Furthermore, instead of vertically passing through membranes, ions and molecules can be forced to permeate through GO-based membranes horizontally. A new device will need to be designed for this idea.

References

[1] Lee, M.; Wu, Z.; Wang, R.; Li, K. *Journal of Membrane Science.* **461**, 39-48 (2014).

[2] Zularisam, A.W.; Ismail, A.F.; Salim, R. *Desalination.* **193**, 211-231 (2006).

[3] Antony, A.; Low, J. H.; Gray, S.; Childress, A. E.; Le-Clech, P.; Leslie, G. *Journal of Membrane Science.* **383**, 1-16 (2011).

[4] Daufin, G.; Escudier, J. P.; Carrere, H.; Berot, S. *Food and Bioproducts Processing.* **79**, 89-102 (2001).

[5] Cassano, A.; Figoli, A.; Tagarelli, A.; Sindona, G.; Drioli, E. *Desalination.* **189**, 21-30 (2006).

[6] Kim, J.; Lee, S.; Srinivasan, S.; Chamberlin, C. E. *Journal of The Electrochemical Society.* **142**, 2670-2674 (1995).

[7] Peighambardoust, S. J.; Rowshanzanmir, S.; Amjadi, M. *International Journal of Hydrogen Energy.* **35**, 9349-9384 (2010).

[8] Baker, R. W. *Industrial & Engineering Chemistry Research.* **41**, 1394-1411 (2002).

[9] Bernardo, P.; Drioli, E.; Gollemme, G. *Industrial & Engineering Chemistry Research.* **48**, 4638-4663 (2009).

[10] Scholes, C. A..; Smith, K. H..; Kentish, S. E.; Stevens, G. W. *International Journal of Greenhouse Gas Control.* **4**, 739-755 (2010).

[11] Huang, H.; Ying Y.; Peng X. *Journal of Materials Chemistry.* **2**, 13772-13782 (2014).

[12] Huang, H.; Mao Y.; Ying Y.; Liu, Y.; Sun, L.; Peng, X. *Chemical Communications.* **49**, 5963-5965 (2013).

[13] Huang, H. *et al. Nature Communications*. **4**, 2979 (2013).

[14] Nakamura, S. *et al. Brain and Development.* **37**, 925-932 (2015).

[15] Fritzmann, C.; Lowenberg, J.; Wintgens, T.; Melin, T. *Desalination.* **216**, 1-76 (2007).

[16] Zhang, Y.; Rhim, J. W.; Feng X. *Journal of Membrane Science.* **444**, 22-31 (2013).

[17] Lakshminarayanaiah, N. *Chemical Reviews*. **65**, 491-565 (1965).

[18] Du, N.; Park, H. B.; Roberston, G. P.; Dal-cin, M. M.; Visser, T.; Scoles, L.; Guiver, M. D. *Nature Materials.* **10**, 372-375 (2011).

[19] Wohr, M.; Bolwin, K.; Schnurnberger, W.; Fischer, M.; Neubrand, W.; Eigenberger, G. *International Journal of Hydrogen Energy.* **23,** 213-218 (1998).

[20] Choi, H.; Stathatos, E.; Dionysiou, D. D. *Applied Catalysis.* **63,** 60-67 (2006).

[21] Hummer, G.; Rasaiah, J. C.; Noworyta, J. P. *Nature.* **414,** 188-190 (2001).

[22] Majumder, M.; Chopra, N.; Hinds, B.J. *ASC Nano.* **5**, 3867-3877 (2011).

[23] Karan, S.; Samistu, S.; Peng, X.; Kurashima, K.; Ichinose, I. *Science.* **335,** 444-447 (2012).

[24] Aisenberg, S.; Chabot, R. *Journal of Applied Physics.* **42,** 2953 (1971).

[25] Joshi, R. K.; Alwarappan, S.; Yoshimura, M.; Sahajwalla, V.; Nishina, Y. *Applied Materials Today.* **1**, 1-12 (2015).

[26] He, H.; Klinowski, J.; Forster, M.; Lerf, A. *Chemical Physics Letters.* **287**, 53-56 (1998).

[27] Nair, R. R.; Wu, H. A.; Jayaram, P. N.; Grigorieva, I. V.; Geim, A. K. *Science*. **335,** 442-444 (2012).

[28] Kim, H. W.; *et al. Science.* **342,** 91-95 (2013).

[29] Li, H.; *et al. Science.* **342,** 95-101 (2013).

[30] Joshi, RK.; Carbone, P.; Wang, F. C.; Kravets, V. G.; Su, Y.; Grigotieva, I. V.; Wu, H. A.; Geim, A. K.; Nair, R. R. *Science.* **343,** 752-754 (2014).

[31] Sun, Z.; Zhu, M.; Wang, K.; Zhong, M.; Wei, J.; Wu, D.; Xu, Z.; Zhu, H. *ACS Nano.* **7,** 428-437 (2013).

[32] Coleman, M.; Tang X. *Nano Research.* **8**, 1128-1138 (2015).

[33] Marcel, M. Basic principles of membrane technology. *Kluwer Academic*. (1996).

[34] Maloney, D. J.; MacDonnell, F. M. *Acta Crystallographica Section C.* **53,** 705-707 (1997).

[35] Rillema, D. P.; Jones, D. S. *J.C.S Chemical Communications.* **412,** 849-851 (1979).

[36] Moret, M.; Tavernelli, I.; Rothlisberger, U. *Journal of Physical Chemistry*. **113,** 7737-7744 (2009).

[37] Mi B. *Science.* **343,** 740-742 (2014).

[38] Boukhvalov, D. W.; Katsnelson, MI.; Son, Y. *Nano Letters.* **13,** 3930-3935 (2013).

[39] Ganesh, B. M.; Isloor, A. M.; Ismail, A. F. *Desalination.* **313,** 199-207 (2013).

[40] Zhu, Y.; Murali, S.; Stoller, M. D.; Ganesh, K.; Cai, W.; Ferreira, P. J.; Pirkle, A.; Wallace, R. M.; Cychosz, K. A.; Thommes. M. *Science.* **332**, 1537-1541 (2011).

[41] Ying, Y.; Sun, L.; Wang, Q.; Fan, Z.; Peng, X.; *RSC Advances.* **4,** 21425-21428 (2014).

[42] Park, S.; Lee, K.-S.; Bozoklu, G.; Cai, W.; Nguyen, S.T.; Ruoff, R.S. *ACS Nano.* **2,** 572-578 (2008).

[43] Yeh, C-N.; Raidongia, K.; Shao, J.; Yang, QH.; Huang, J. *Nature Chemistry.* **7**, 166-170 (2015).

[44] Cheng, Q.; Wu, M.; Li, M.; Jiang, L.; Tang, Z. *Angewandte Chemie International Edition.* **52,** 3750-3755 (2013).

[45] Hu, M.; Mi, B. *Environmental Science and Technology.* **47**, 3715-3723 (2013).

[46] O'Hern, S.; Boutulier, M.; Idrobo, J-C.; Song, Y.; Kong, J.; Laouli, T.; Atiehl, M.; Karnlk, R. *Nano Letters.* **14,**1234-1241 (2014).

[47] Sun, P.; Liu, H.; Wang, K.; Zhong, M.; Wu, D.; Zhu, H. *Chemical Communications.* **51,** 3251-3254 (2015).

[48] Cohen-Tanugi, D.; Grossman, J. *Nano Letters.* **12**, 3602-2608 (2012).

[49] Hummers, W.; Offeman, R. *Journal of American Chemical Society.* **80,** 1339-1340 (1958).

[50] Gao, X.; Tang, X. S. *Carbon.* **76**, 133-140 (2014).

[51] Raidongia, K.; Huang, J. *Journal of the American Chemical Society.* **134,** 16528-16531 (2012).

[52] Yang, H.; Hu, H.; Wang, Y.; Yu, T. *Carbon.* **52,** 528-534. (2013).

[53] Ai, K.; Liu, Y.; Cheng, X.; Huo, L. *Journal of Material Chemistry.* **21,** 3365-3370 (2011).

[54] Sun, X. *Nano Research.* **1**, 203-211 (2008).

[55] Yang, S.; Yue, W.; Huang, D.; Chen, C.; Lin, H.; Yang, X. *RSC Advances*. **2**, 8827-8832 (2012).

[56] Paredes, J. I.; Villar-Rodil, S.; Martinez-Alonso, A. *American Chemical Society.* **24**, 10560-10564 (2008).

[57] Nghiem, L.D.; Schafer. A. I.; Elimelech, M. *Environmental Science Technology.* **38**, 1888-1896 (2004).

[58] Yaroshchuk, A. E. *Journal of Membrane Science.* **239**, 9-15 (2004).

[59] Bellona, C.; Drewes, J.E.; Xu, P.; Amy, G. *Water Research.* **38**, 2795-2809. (2004).

[60] Hilal, N.; Al-Zoubi, H.; Darwish, N. A.; Mohamma, A. W. *Desalination.* **170**, 281-308 (2004).

[61] Causserand, C.; Aimar, P.; Vilani, C.; Zambelli, T. *Desalination.* **149,** 485-491 (2002).

[62] Geens, J.; Van der Bruggen, B.; Vandecasteele, C. *Separation and Purification Technology.* **48,** 255-263 (2006).

[63] Tanyra, M.; Jyrata, M.; Odani, H.; Bull. *Chemical Society of Japan.* **28,** 83 (1955).

[64] Park, S. M.; Choi, Y.; Lee, S.; Baek, Y.; Yoon, J.; Seo, D. K.; Kim, Y. H. *Desalination and Water Treatment.* **51**, 5349-5354 (2013).

[65] Marchetti, P.; Butte, A.; Livingston, A. G. *Journal of Membrane Science.* **415-416,** 444 (2012).

[66] Tanardi, C. R.; Vankelecom, I. F. J.; Pinheiro, A. F. M.; Kishore, K. R.; Nijmeijer, A.; Winnubst, L. *Journal of Membrane Science.* **495**, 216-225 (2015).

[67] Raman, L. P.; Cheryan, M.; Rajagopalan, N. *Chemical Engineering Progress.* **90**, 68-74(1994).

[68] Bowen, W. R.; Welfoot, J. S. *Chemical Engineering Science.* **57**, 1121-1137 (2002).

[69] Geens, J.; Peeters, K.; Bruggen, B. V.; Vandecasteele, C. *Journal of Membrane Science.* **255,** 255-264 (2005).

[70] Dikin, D. A.; Stankpvich, S.; Zimney, E. J.; Piner, R. D.; Dommett, G. B.; Evmenenko, G.; Nguyen, S. T.; Ruoff, R.S. *Nature.* **448,** 457-460 (2007).

[71] Tang, Y. P.; Paul. D. R.; Chung, T. S. *Journal of Membrane Science.* **458,** 199-208 (2014).

[72] Khattab, I. S.; Bandarkar, F.; Fakhree, M. A. A.; Jouyban, A. *Journal of Chemical Engineer.* **29**, 812-817 (2012).

[73] Huang, K.; Liu, G.; Lou, Y.; Dong, Z.; Shen, J.; Jin, W. *Angewandte Chemie International Edition.* **53,** 6929-6932 (2014).

[74] Qiu, L.; Zhang, X.; Yang, W.; Wang, Y.; Simon, G.; Li, D. *Chemical Communications.* **47,** 5810-5812 (2011).

[75] Han, Y.; Xu, Z.; Gao, C. *Advanced Functional Materials.* **23**, 3693-3700 (2013).

[76] Goh, K.; Setiawan, L.; Wei, L.; Si, R.; Fane, A. G.; Wang, R.; Chen Y. *Journal of Membranes Science.* **474,** 244-253 (2015).

[77] Bowen, W. R.; Cassey, B.; Jones, P.; Oatley, D. L. *Journal of Membrane Science.* **242**, 211-220 (2004).

[78] Chi, C.; Wang, X.; Peng, Y.; Qian, Y.; Hu, Z.; Dong, J.; Zhao, D. *Chemistry of Materials.* **28,** 2921-2927 (2016).

[79] Hu, Y.; Wei, J.; Liang, Y.; Zhang, H.; Zhang, X.; Shen, W.; Wang, H. *Angewandte Chemie International Edition.* **55**, 2048-2052 (2016).

[80] Baradaran, S.; Moghaddam, E.; Basirun, W. J.; Mehrail, M.; Sookhakian, M.; Hamdi, M.; Moghaddam, M. R. N.; Alias, Y. *Carbon.* **69,** 32-45 (2014).

[81] Ramanathan, T.; *et al. Nature Nanotech.* **3**, 327-332 (2008).

[82] Xu, Z.; Zhang, J.; Shan, M.; Li, Y.; Li, B.; Niu, J.; Zhou, B.; Qian, X. *Journal of Membrane Science.* **458,** 1-13 (2014).

[83] Mahmoud, K. A.; Mansoor, B.; Mansour, A. M.; Khraisheh, M. *Desalination.* **356,** 208-225 (2015).

[84] Wang, S.; Zhang, D.; Ni, X. *Chinese Journal of Polymer Science*. **34**, 805-819 (2016).

[85] Qu, X.; Alvarez, P. J.; Li, Q. *Environmental Science and Technology.* 47, 3931-3946 (2013).

[86] Machado, D. R.; Hasson, D.; Semiat, R. *Journal of Membrane Science*. **166,** 63-69 (2000).

[87] Bruggen, B. V.; Geens, J.; Vandecasteele, C. *Chemical Engineering Science.* **57**, 2511-2518 (2002).

[88] Nghiem, L. D.; Schafer, A.I.; Elimelech, M. *Environmental Science and Technology.* **36,** 1888-1896 (2004).

[89] White, L. S. *Journal of Membrane Science*. **205,** 191-202 (2002).

[90] Bhanushali, D.; Kloos, S.; Bhattacharyya, D. *Journal of Membrane Science*. **208,** 343-359 (2002).

[91] Reid, R. C.; Prausnitz, J. M. *The properties of gases and liquids. McGraw-Hill*, New York (1977).

[92] Wilke, C. R.; Chang, P. *American Institute of Chemical Engineers.* **1,** 264-270 (1955)

[93] Scheibel, E. G. *Industrial and Engineering Chemistry.* **46,** 2007 (1954)

[94] Lusis, M. A.; Ratcliff, G.A. *Canadian Journal of Chemical Engineering.* **46,** 385 (1968)

[95] Gornshteyn, B. J. *The Canadian Journal of Chemical Engineering.* **81**, 139-146 (2003).

[96] Harris, K. R. *The Journal of Chemical Physics.* **132**,231103 (2010).

[97] Kamaruddin, D.; Koros, W.J. *Journal of Membrane Science.* **135,** 147-159 (1997).

[98] Guo, W.; Cheng, C.; Wu, Y.; Jiang, Y.; Gao, J.; Li, D.; Jiang, L. *Advanced Materials.* **25**, 6064-6068 (2013).

[99] Kuila, T.; Bose, S.; Mishra, A.; Khanra, P.; Jim, N.; Lee, J. *Progress in Materials Science.* **57,** 1061-1105 (2012).

[100] Georgakilas, V.; *et al. Chemical Reviews.* **112**, 6156-6214 (2012).

[101] Tasis, D.; Tagmatarchis, N.; Biaoncao, A.; Parto, M. *Chemical Reviews.* **106,** 1105-1136 (2006).

[102] Wu, J.; Zhan, X.; Hinds, B. *Chemical Communications.* **48**, 7979-7981 (2012).

[103] Mapkar, J.A.; Lyer, G.; Coleman, M. *Applied Surface Science.* **9,** 4806-4813 (2009).

[104] O'hern, S.; Boutilier, M.; Idrobo, J-C.; Song, Y.; Kong, J.; Laouli, T.; Atiehl, M.; Karnik, R. *Nano Letters.* **14**, 1234-1241 (2014).

[105] Tasaki, K. *Journal of the American Chemical Society.* **118**, 8459-8469 (1996).

[106] Oelmeier, S.; Dismer, F.; Hubbuch, J. *Biophysics.* **5**, 14-28 (2012).

[107] Jiang, D.; Cooper, V.; Dai, S. *Nanoletters.* **12**, 4019-4024 (2009).

[108] Lu, T.; Zhang, Y,P.; Li, H, B.; Pan, L. *Electrochimica ACTA.* **55**, 4170 (2010).

[109] Wang, D,H.; *et al. ACS Nano.* **4**, 1587 (2010).

[110] Kou, R.; *et al. Electrochemistry Communications.* **11**, 954 (2009).

[111] Liu, H.; Gao, J.; Xue, M.; Zhu, N.; Zhang, M.; Cao, T. *Langmuir.* **25,** 12006 (2009).

[112] Zu, S, Z.; Han, B. H. *Journal of Physical Chemistry*. **113,** 13651 (2009).

[113] Chen, D.; Feng, H.; Li, J. *Chemical Reviews.* **112,** 6027-6053 (2012).

[114] Wei, N.; Peng, X.; Xu, Z. *Physical Review E*. **89**, 012113 (2014).

[115] A, Wakisaka.; K, Matsuura. *Journal of Molecular Liquids.* **129**, 25-32 (2006).

[116] M, Soltesova.; L, Benda.; Peksa, M.; Czernek, J.; Lang, J. *Journal of Physical Chemistry.* **118,** 6864-6874 (2014).

Appendix A

Index Refraction

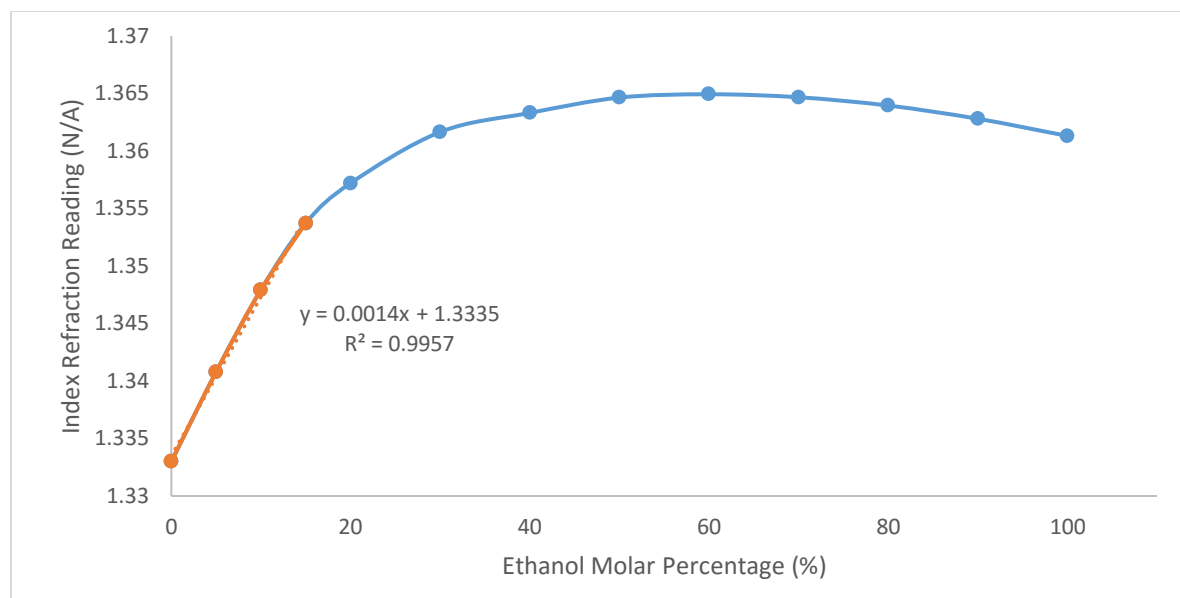| Mole% Ethanol (%)	Mole% Water (%)	V_E/V_W (No unit)	Index Refraction Reading
0	100	0	1.3330
5	95	0.1707	1.3408
10	90	0.3604	1.3479
15	85	0.5725	1.3537
20	80	0.8110	1.3572
30	70	1.3903	1.3617
40	60	2.1626	1.3633
50	50	3.2439	1.3646
60	40	4.8659	1.3649
70	30	7.5692	1.3646
80	20	12.9758	1.3640
90	10	29.1955	1.3628
100	0	All Ethanol	1.3613

Table A1. Index refraction of water/ethanol mixture.

Figure A1. Index refraction calibration curve of water/ethanol mixtures

The index refraction calibration curve shows perfect linear property only in the low ethanol molar percentage range (0% - 15%), but the index refraction readings keep monotonic with ethanol molar percentages under 30% ethanol. Therefore, our solvent mixture transport experiments focused on separation performance of GO membranes towards ethanol/waterloo mixtures with ethanol molar percentage no greater than 30%. For the measurements in the range of 15% - 30% ethanol, ethanol molar percentages were determined by fitting the readings into the calibration curve.

Appendix B

Tris(2,2-bipyridyl) dichlororuthenium(II) hexahydrate

Ru(bpy)$_3^{2+}$ ion transport through

GO-based membranes
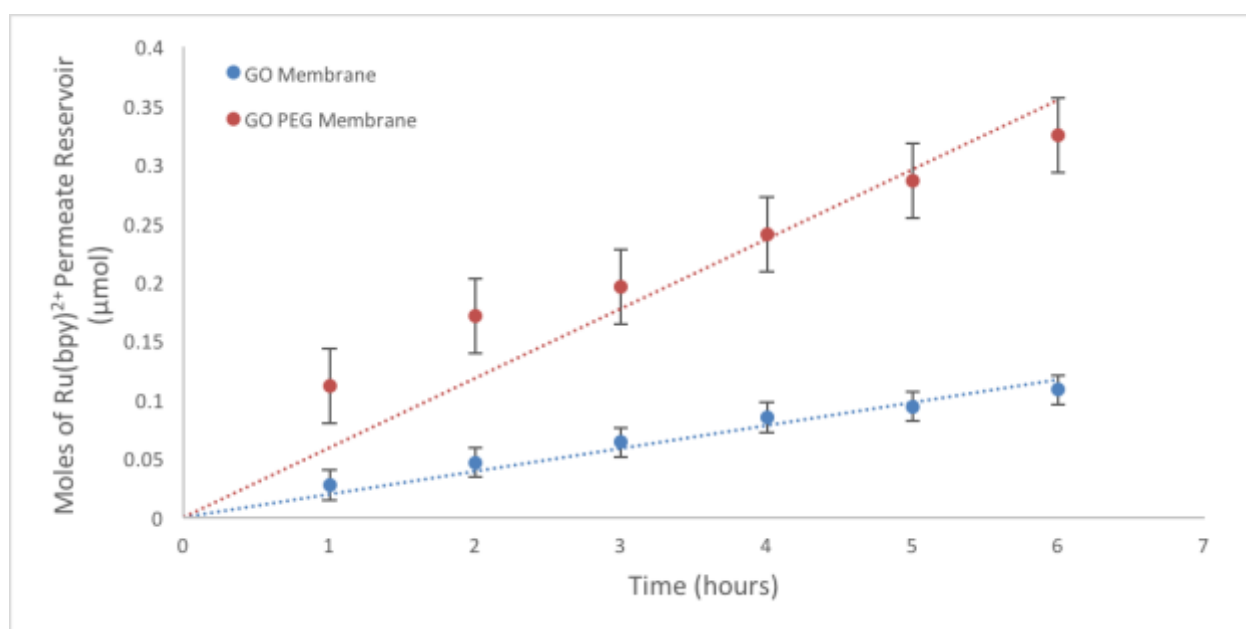

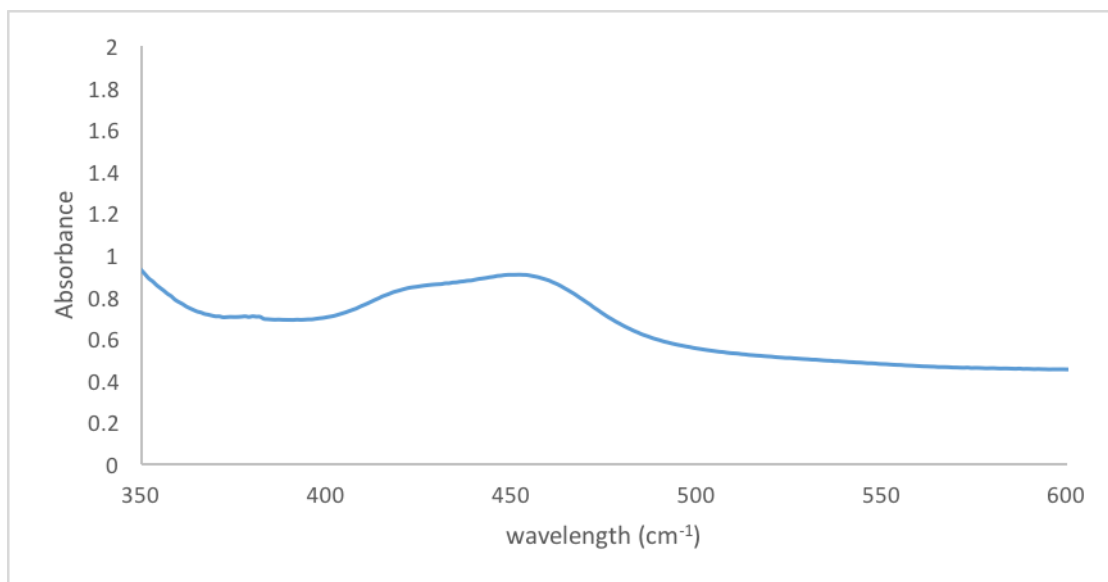Figure B1. Moles of Ru(bpy)$_3^{2+}$ ions transported through GO, and PEG-GO membranes over 6 hours.

Figure B2. UV-Vis spectrum of Ru(bpy)$_3$$^{2+}$ in water solution.
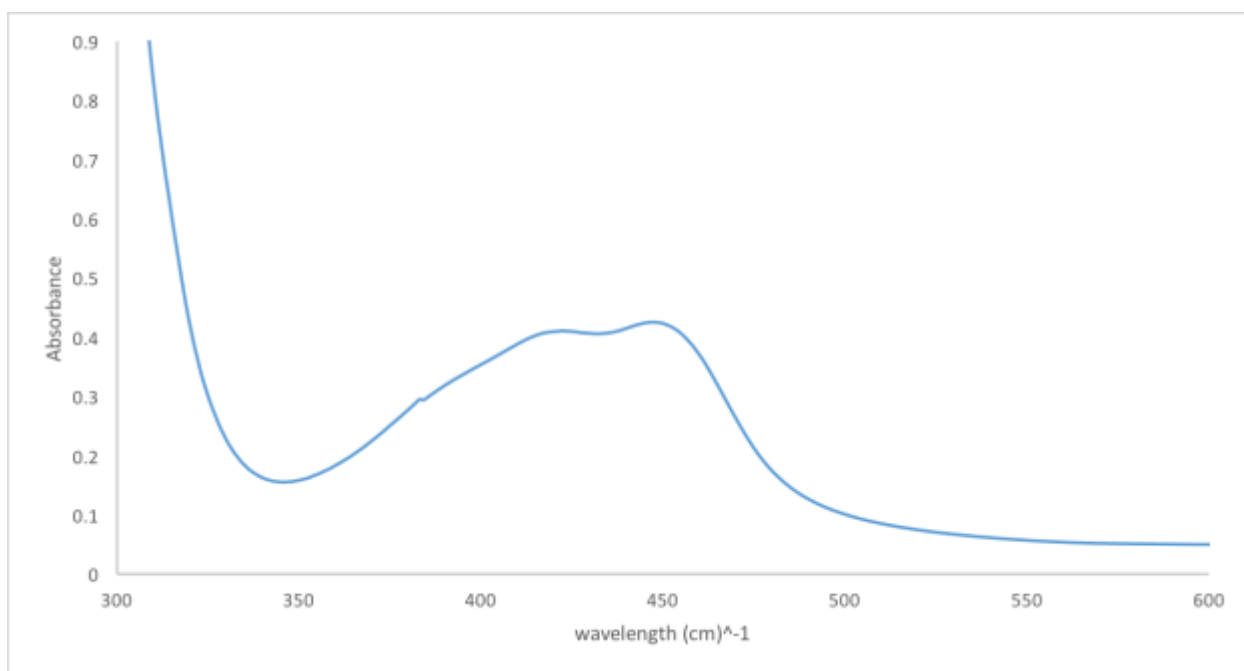

Figure B3. UV-Vis spectrum of Ru(phen)$_3$$^{2+}$ in water solution.